Metadata of the chapter that will be visualized online

Chapter Title	Myosin and Actin Filaments in Muscle: Structures and Interactions	
Copyright Year	2017	
Copyright Holder	Springer International Publishing AG	
Corresponding Author	Family Name	**Squire**
	Particle	
	Given Name	**John M.**
	Suffix	
	Division	School of Physiology, Pharmacology & Neuroscience
	Organization/University	University of Bristol
	Address	Bristol, BS8 1TD, UK
Author	Family Name	**Paul**
	Particle	
	Given Name	**Danielle M.**
	Suffix	
	Division	School of Physiology, Pharmacology & Neuroscience
	Organization/University	University of Bristol
	Address	Bristol, BS8 1TD, UK
Author	Family Name	**Morris**
	Particle	
	Given Name	**Edward P.**
	Suffix	
	Division	Division of Structural Biology
	Organization/University	The Institute of Cancer Research
	Address	London, SW3 6JB, UK

Abstract	In the last decade, improvements in electron microscopy and image processing have permitted significantly higher resolutions to be achieved (sometimes <1 nm) when studying isolated actin and myosin filaments. In the case of actin filaments, the changing structure when troponin binds calcium ions can be followed using electron microscopy and single particle analysis to reveal what happens on each of the seven non-equivalent pseudo-repeats of the tropomyosin α-helical coiled-coil. In the case of the known family of myosin filaments, not only are the myosin head arrangements under relaxing conditions being defined, but the latest analysis, also using single particle methods, is starting to reveal the way that the α-helical coiled-coil myosin rods are packed to give the filament backbones.
Keywords (separated by " - ")	

Chapter 11
Myosin and Actin Filaments in Muscle: Structures and Interactions

John M. Squire, Danielle M. Paul, and Edward P. Morris

Contents

Abstract In the last decade, improvements in electron microscopy and image processing have permitted significantly higher resolutions to be achieved (sometimes <1 nm) when studying isolated actin and myosin filaments. In the case of actin fila-

J.M. Squire (✉) • D.M. Paul
School of Physiology, Pharmacology & Neuroscience, University of Bristol,
Bristol BS8 1TD, UK
e-mail: j.squire@imperial.ac.uk

E.P. Morris
Division of Structural Biology, The Institute of Cancer Research, London SW3 6JB, UK

33 ments, the changing structure when troponin binds calcium ions can be followed
34 using electron microscopy and single particle analysis to reveal what happens on
35 each of the seven non-equivalent pseudo-repeats of the tropomyosin α-helical
36 coiled-coil. In the case of the known family of myosin filaments, not only are the
37 myosin head arrangements under relaxing conditions being defined, but the latest
38 analysis, also using single particle methods, is starting to reveal the way that the
39 α-helical coiled-coil myosin rods are packed to give the filament backbones.

40 **Keywords** Muscle thick filaments • Titin • Tropomyosin • Myosin binding protein-
41 C • C-protein • Myosin rod packing • Paramyosin • Troponin • Nebulin

42 ## 11.1   Introduction and Overview of the Sarcomere

43 Myosin and actin filaments are most abundant in muscle, where they form the sar-
44 comere in the striated muscles of vertebrates and invertebrates and the less ordered
45 contractile units in vertebrate and molluscan smooth muscles (Squire 1981). After
46 the discovery of the sliding filament mechanism in muscle by Huxley and Hanson
47 (1953) and Huxley and Niedergerke (1953), which suggested that the sarcomere
48 contains separate overlapping sets of thick and thin filaments (Fig. 11.1a middle),
49 each of which remain more or less constant in length, a concentrated effort was
50 made over the next few years towards defining the nature of these filaments. It was
51 Hugh Huxley (1963) who first showed that the thick filaments contain myosin mol-
52 ecules, which are long rod-shaped molecules with a globular region at one end
53 (Fig. 11.1a; top). He found that these molecules pack together with their rods anti-
54 parallel in the middle of a myosin filament and parallel towards each end, with the
55 globular regions of the myosin molecules arrayed on the filament surface
56 (Fig. 11.1a). Vertebrate muscle myosin filaments are bipolar; a 180° rotation around
57 an axis perpendicular to the long axis of the filament and halfway along its length
58 would leave the filament looking unchanged.

Fig. 11.1 (continued) end, aggregate to form the myosin filament backbone (*green*) with the myo-
sin heads (*yellow*) arrayed on the filament surface in a helical or quasi-helical array. Actin filaments
(*lower image*) contain actin monomers (*grey spheres*) together with strands of tropomyosin (blue
lines) and troponin (*blue sphere*) (Adapted from Squire et al. 2005) (**b**) Summary of the biochemi-
cal cycle of adenosine triphosphate (ATP) hydrolysis by myosin (M) and actin (A) as proposed by
Lymn and Taylor (1971). ATP hydrolysis occurs with myosin detached from actin (M.ATP to
M.ADP.Pi). ADP is adenosine diphosphate. M.ADP.Pi attaches to actin and while attached Pi
(inorganic phosphate) and then ADP are released during which aat some point force and movement
are generated. Further binding of ATP to the myosin heads causes head detachment from actin
(Adapted from Squire et al. 2005)
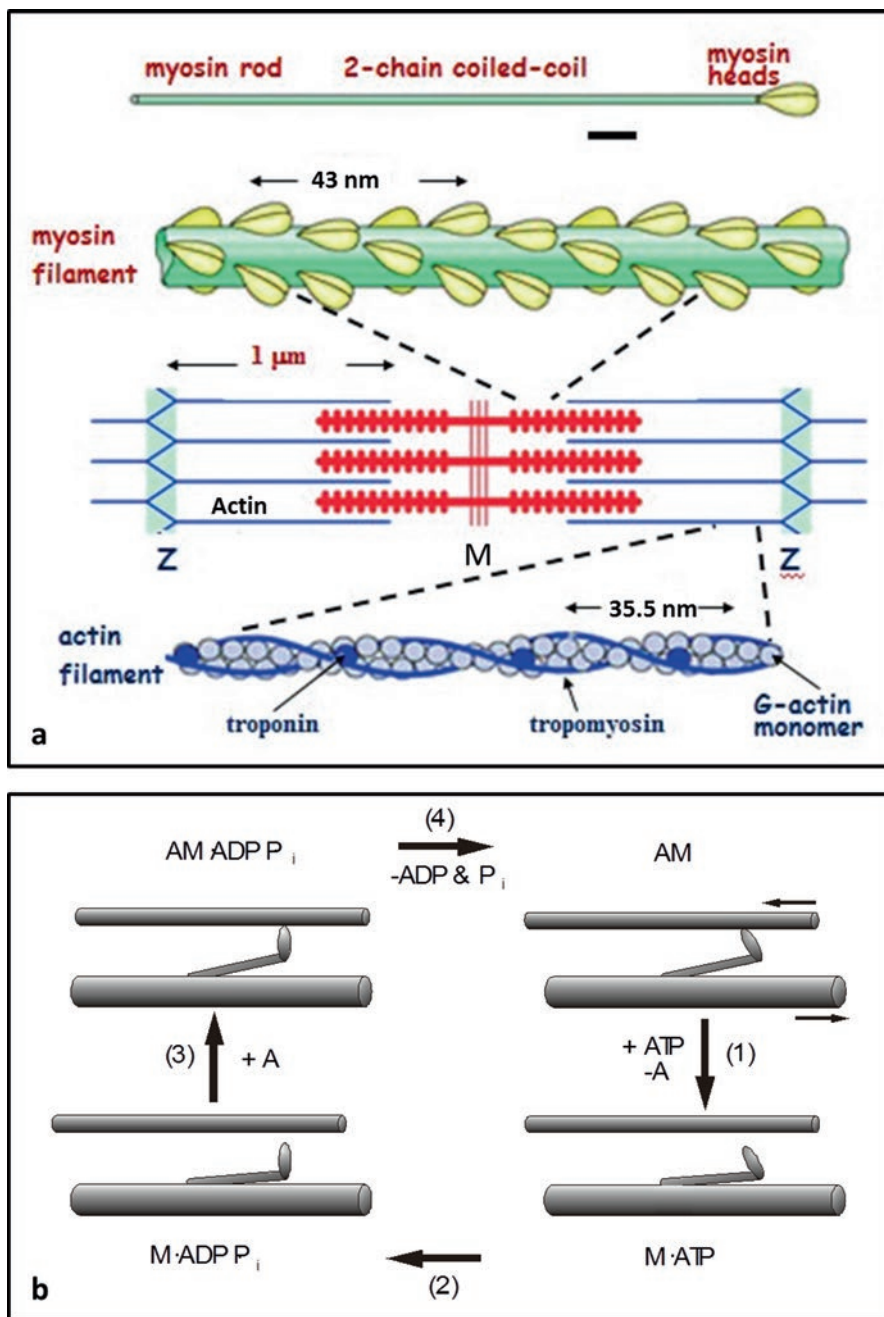
Fig. 11.1 (**a**) Schematic drawings of a striated muscle sarcomere (*central image*) showing overlapping myosin filaments (*red*) centred on the M-band (M) and actin filaments anchored to the Z-line (Z). Myosin rods (*top*), two-chain α–helical rods with two globular domains (heads) at one

The basic structure of actin filaments was first visualised by Hanson and Lowy (1963) using electron microscopy of isolated actin filaments viewed in negative stain. Actin filaments were seen to look like two strands of beads twisting around each other (Fig. 11.1a lower figure). The precise dimensions of these filaments were contentious, but by the time of the publication of the monumental X-ray diffraction study of frog *sartorius* muscle by Huxley and Brown (1967) the actin filaments were thought to be helical with a long repeat of around 35–36 nm and containing roughly 13 actin subunits in six turns of the genetic helix. In this same paper it was proposed that the myosin heads on the myosin filaments in frog muscle were arranged on a 2-start helix, with a subunit axial translation of 14.3 nm (the characteristic axial spacing of all types of myosin filament) and a true repeat after about 43 nm.

In the vertebrate striated muscle sarcomere (Fig. 11.1a; middle), the myosin filaments, cross-linked at their centres by M-band proteins, define the A-band (e.g. see Squire et al. 2005). They are overlapped at each end by actin filament arrays of opposite polarity, emanating from the Z-bands at the sarcomere edges. In cross-section, the myosin filaments form a hexagonal array, and in vertebrate striated muscles the actin filaments are located at the middle of a triangle formed by three adjacent myosin filaments (the so-called trigonal point).

It was also found early on that the globular part of myosin seen by Huxley was actually two globular domains, known as the myosin heads, on the end of a 150 nm long two-chain coiled-coil α–helical myosin rod (Slayter and Lowey 1967; Lowey et al. 1969; Fig. 11.1a top). These heads are ATPases, which can bind to actin, especially strongly in the absence of ATP, and the myosin head ATPase is activated by the interaction with actin. An early idea (e.g. Huxley 1969) was then that the myosin heads would bind reversibly to actin during muscle contraction in a cycle powered by ATP and that, when attached to actin, the heads would change their configuration on actin in some way, thereby producing movement (Fig. 11.1b; Huxley 1969; Lymn and Taylor 1971). But how was the muscle switched on? Early work had shown that tropomyosin, another two-chain coiled-coil α–helical protein, was associated with actin filaments. Then, in a ground-breaking study, Ebashi and his colleagues (Ebashi and Endo 1968) discovered the protein troponin on actin filaments in muscle, a protein which would reversibly bind calcium ions in the physiological range of calcium concentrations. In this scenario, an electrical stimulus travelling down the muscle nerve and into the t-tubular system would cause the release of calcium ions from the sarcoplasmic troponin on the actin filaments and, somehow, the actin filaments would be switched on.

The mechanism of switching was the subject of painstaking X-ray diffraction work by two groups, Hugh Huxley and his colleagues in Cambridge, England (Huxley 1972) and Peter Vibert and his colleagues in Aarhus, Denmark (Vibert et al. 1972). What they found was very striking. X-ray diffraction patterns from the actin filaments in muscle are characterised by so-called layer lines (Fig. 11.2, horizontal lines of spots) with positions (spacings) that are orders of the basic actin filament axial repeat of around 35.5 nm. The first layer line corresponds to a repeat of 35.5 nm, the 2nd layer line to a spacing of 17.8 nm, the 3rd to a spacing of 11.8 nm
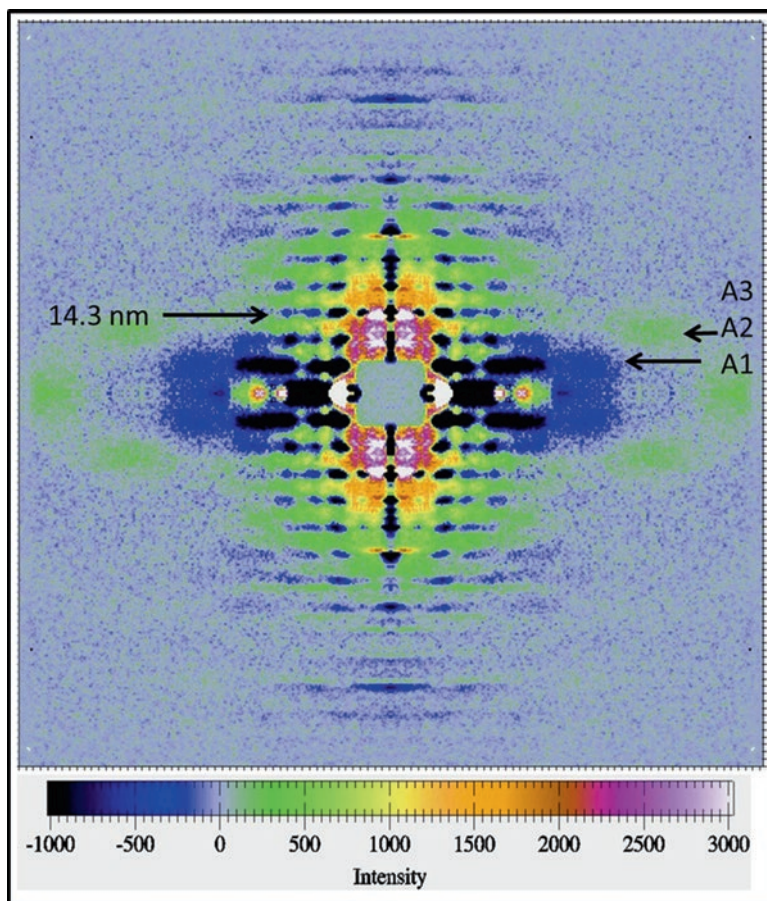
Fig. 11.2 Low-angle X-ray diffraction pattern from a vertebrate striated muscle (*fish muscle*) oriented with its long axis up the page and shown as a difference intensity map of the pattern from relaxed muscle subtracted from the pattern from fully active muscle (plateau of an isometric tetanic contraction). The key at the bottom shows how increases and decreases are depicted in the difference pattern. Of particular note is the increase in intensity (*green*) of the 2nd actin layer line (A2) in patterns from active muscle. The 3rd myosin layer line at 14.3 nm is also indicated (Modified from Mok 2005)

and so on. These authors found that in X-ray diffraction patterns from resting mus-   104
cle the 2nd layer line was relatively weaker than the 3rd, whereas in patterns from   105
active muscle the 2nd layer line became much stronger, overtaking the 3rd which,   106
in turn, became weaker. Figure 11.2 shows such changes in a more recent study and   107
are illustrated as a difference map showing which layer lines change (Mok 2005).   108

What did these changes mean? Ebashi had already suggested that tropomyosin   109
molecules might lie along the grooves of the actin helix, with a troponin complex on   110
each tropomyosin molecule. The tropomyosin molecules are about 40 nm long and   111
would cover about seven actin subunits. We know that calcium ions would bind to   112
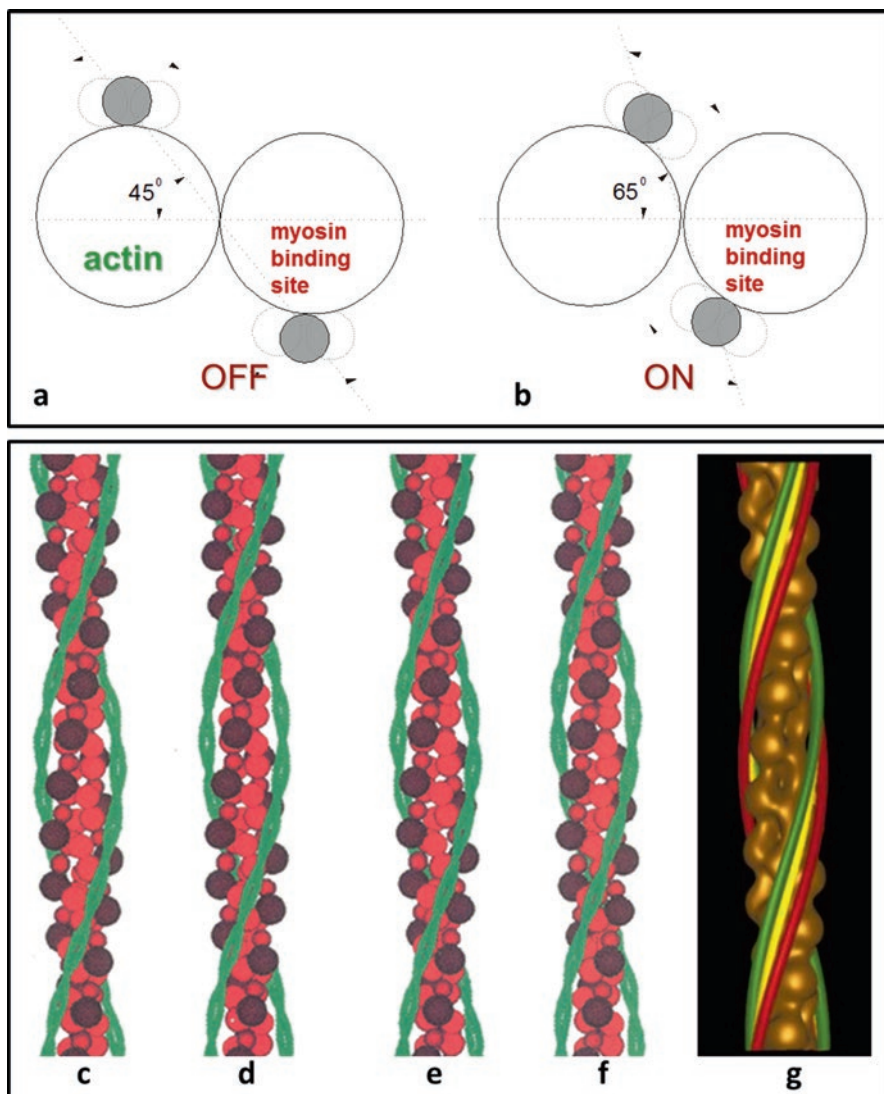
Fig. 11.3 (**a**, **b**) Illustration of the steric blocking model of muscle regulation as depicted in Parry and Squire (1973). The two strands of actin monomers are shown in cross-section as large circles. The small *grey circles* show the position of the tropomyosin strands under different conditions. In relaxed muscle (**a**, off, low calcium) the tropomyosins are well out of the grooves between the two actin strands. With elevated calcium levels (**b**), causing calcium binding to troponin, the tropomyosin strands move in towards the groove, thus uncovering the myosin binding sites on actin. The small *hollow circles* show the possible extent of small oscillations of the tropomyosin strands around their preferred location. It is as well to remember that the structure will never be static. Adapted and modified from Parry and Squire (1973). (**c** to **f**) Interleaved stereo pairs of a model

Fig. 11.4 3D reconstruction of actin filaments labelled with myosin heads in the absence of ATP showing the characteristic arrowhead structure and revealing where on actin the myosin heads bind
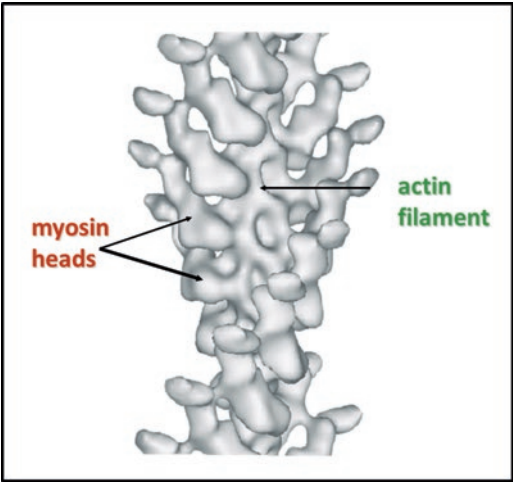
troponin in active muscle, but why would the layer lines change? The answer was shown at the same time by Huxley (1972), Haselgrove (1972) and Parry and Squire (1973). They found that tropomyosin strands were not actually right in the grooves of the actin filament in resting muscle, but were displaced laterally from the middle of the grooves (Fig. 11.3a, c, e). It was suggested that their position in resting muscle was such that the tropomyosin would block myosin head attachment, either directly or indirectly, so that contraction could not occur (Fig. 11.3a). As discussed later, the myosin head position on actin had been determined by electron microscopy and image processing of actin filaments labelled with myosin heads in the rigor state (Moore et al. 1970; a more recent structure is shown in Fig. 11.4).

When calcium ions became bound to troponin in active muscle, the effect seemed to be to move the tropomyosin strands closer to the grooves of the actin filaments, thereby exposing the myosin binding sites on actin (Fig. 11.3b, d, f). This mechanism became known as the 'Steric Blocking Mechanism'. All these authors showed that this movement probably occurred, but Parry and Squire (1973) also showed that every other type of movement of tropomyosin that they could think of failed to explain the observations; the tropomyosin shift appeared to be the only change possible. They also showed that tropomyosin molecules have a periodic repeat along them which divided the molecules into seven or 14 repeats (confirmed by Parry

Fig. 11.3 (continued) actin filament showing tropomyosin strands (*green*) in the off position (**c** and **e**) and in the on position (**d** and **f**). The actin monomers are represented as four spheres in various shades of *red* (cf Fig. 11.5a). (**g**) Results based on 3D reconstructions of actin filaments in various states showing the three positions of tropomyosin associated with the off (*red*), calcium activated (*yellow*) and myosin head-bound (*green*) positions of tropomyosin ((**c**–**f**) from Squire and Morris 1998. (**g**) Reproduced from Craig and Lehman (2001) with permission)

132 1975; McLachlan and Stewart 1976), supporting an earlier conclusion from X-ray
133 diffraction from tropomyosin tactoids (Caspar et al. 1969). The axial repeat of tro-
134 ponin on the actin filaments was about 38.5 nm (Huxley and Brown 1967), so 38.5/7
135 = 5.5 nm coincided with the axial separation of actin monomers along one long
136 pitched strand of actin; one tropomyosin molecule could make similar (not identi-
137 cal) interactions with seven actin monomers. The regulatory unit in the thin filament
138 was, therefore, seven actin monomers, one tropomyosin molecule and one troponin
139 complex, as originally suggested by Ebashi and Endo (1968).
140 With these basic ideas about myosin and actin filaments established, structural
141 studies of both filaments types since the early 1970s have progressed in gradually
142 improving steps dictated by the available techniques. Here we briefly describe the
143 methods used and the results that have been obtained.

11.2 Actin Filament Structure

11.2.1 3D Reconstruction of Actin Filaments

146 The first big step forward came from the realisation that electron micrograph images
147 of extended helical objects, like actin filaments, lying down on the electron micro-
148 scope grid actually contain many views of the same object, but at different rotations
149 (i.e. viewing angles) around the long axis of the objects. We know that being able to
150 view objects with our own two eyes means that we get a 3D impression of those
151 objects. Therefore, a single image of a helical object in the electron microscope
152 presenting many different views of the same object ought to contain the information
153 necessary to reconstruct the object in 3D. Aaron Klug and his colleagues worked
154 out how to do this using the computed Fourier transform of the object in an electron
155 micrograph (DeRosier and Klug 1968), and this technique was put to good use on
156 helical actin filaments by Moore et al. (1970), see also DeRosier and Moore (1971).
157 The method was particularly useful when applied to actin filaments with myosin
158 heads bound in the absence of ATP (Fig. 11.4). Here the curved, angled, elongated
159 myosin heads were seen to produce a characteristic 'arrowhead' appearance, an
160 appearance that has since been used to define actin filament polarity in a variety of
161 studies. The reconstruction also showed where on actin the myosin heads appeared
162 to bind, and it was this position that enabled the 'steric blocking model', mentioned
163 earlier, to suggest that 'off' state tropomyosin was in the right place to block myosin
164 head attachment.

11.2.2 Checking the Steric Blocking Model

166 The early X-ray diffraction evidence for the steric blocking model was itself fairly
167 compelling. However, it is always good to be able to see structures directly. In a
168 series of papers, Roger Craig, William Lehman, Peter Vibert and their colleagues

(Lehman et al. 1994, 1995; Vibert et al. 1997) studied actin / tropomyosin / troponin structures in a variety of states and from different muscles using the helical reconstruction method of Moore et al. (1970). Use was made of the roughly 13/6 helical symmetry of the actin filaments so that every actin monomer, together with its tropomyosin sub-repeat, was averaged together. It was known from the start that this was an approximation, since the seven tropomyosin sub-repeats in one molecule are not identical. But it was a good starting point and the result was that tropomyosin strands were seen in three different positions on actin (Fig. 11.3g); see Vibert et al. 1997 and many references therein). The three states were the 'off' state, thought to be where myosin head attachment was almost completely blocked, an intermediate state which resulted from calcium activation of the thin filaments, where the tropomyosin had shifted laterally as expected (about 20° rotation around the actin filament axis from the off state), and a third position, another 10° rotated, which resulted when myosin heads were bound in a strong state (e.g. rigor, AM; Fig. 11.1b). These three states were identified by Lehrer and Morris (1982) with the "off", "on" and "potentiated" states characterised by Bremel and Weber (1972). Further work substantiated these states (Phillips et al. 1986; McKillop and Geeves 1993, AL-Khayat et al. AL-Khayat et al. 1995; Brown and Cohen 2005; Poole et al. 2006). The states became known as the Blocked or 'B' state, the closed or 'C' state, where a limited amount of head binding could occur, and the fully open Myosin or 'M' state. Kinetic data were consistent with the tropomyosin being in different equilibria between the states, depending on the conditions (McKillop and Geeves 1993; Lehrer and Geeves 1998).

### 11.2.3   X-Ray Crystallography of Actin and Myosin

Actin filaments occur not just in muscle, but are fundamentally important in all cell types, so when Kabsch et al. (1990) solved the structure of the globular actin (G-actin) monomer by X-ray crystallography, the muscle and cell motility fields were advanced in a spectacular way. The G-actin monomer was found to have four domains in two pairs with a cleft between them, with ATP bound in the bottom of the cleft (Fig. 11.5a). With this structure to hand, and using high angle X-ray diffraction data from oriented gels of actin filaments, Holmes et al. (1990) were then able to suggest how these G-actin molecules might aggregate to form an actin filament (Fig. 11.5c). In brief, subdomains 3 and 4 are closest to the actin filament axis, where they interact with actin monomers in the other strand of the filament, and subdomains 1 (large) and 2 (small) lie on the outside of the filament. Subdomain 1 provides the major binding site for myosin heads. The earlier helical reconstruction work probing the location of tropomyosin in different states also put tropomyosin in the 'off' state binding to subdomain 1 of actin where the heads want to attach.

The field took another major leap forward when the myosin head was crystallised for the first time and its structure determined using X-ray crystallography by Rayment et al. (1993a, b). This showed the head to be a remarkably interesting

AU1

Fig. 11.5 (**a**) Actin monomer with each of its four structural subdomains shown in different colours, subdomain 1: *red*, subdomain 2: *green*, subdomain 3: *blue*, and subdomain 4: *yellow*. (**b**) Schematic of the whole troponin complex with a globular region composed of Tn-C, Tn-I and part of Tn-T (Tn-T2: residues 159-259) with a rod region of Tn-T (Tn-T1: residues 1-158). The crystal structure of Tn-C is shown (Herzberg and James 1988). (**c**) The helical arrangement of the actin monomers along the actin filament, F-actin, according to Holmes et al. (1990). (**d**) Tropomyosin molecules consist of a two-chain α-helical coiled coil (Diagram modified from Squire and Morris 1998)
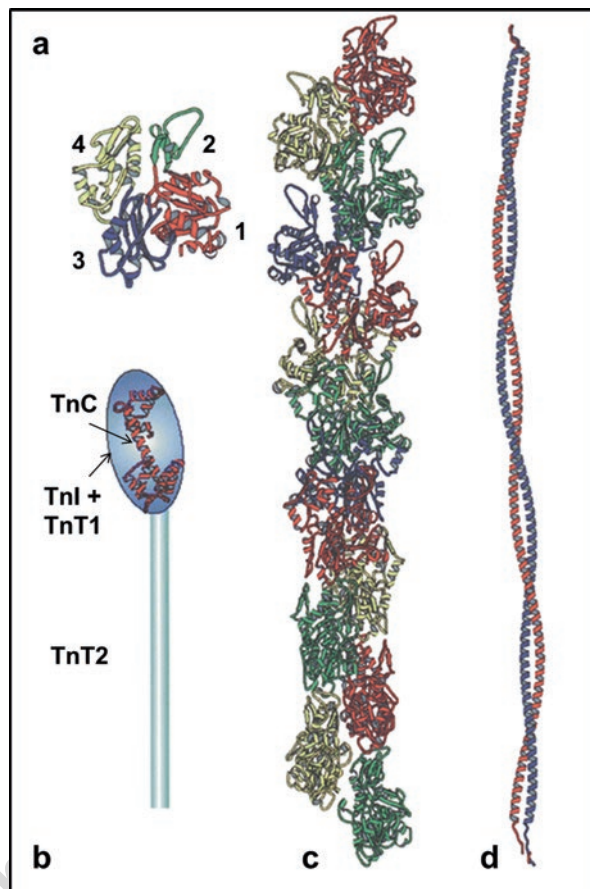
structure (Fig. 11.6a). It consists of a motor domain, which contains the ATPase site, and the part of the head that binds to actin. This is then linked through a so-called converter domain to a long α-helical region around which wrap two myosin light chains, the essential light chain (ELC) and the regulatory light chain (RLC). This region is called the tail or lever arm of the myosin head. It was then found that, with different ATP analogues bound to the heads (Rayment et al. 1993b; Dominguez et al. 1998; Houdusse et al. 2000), the motor domain remained fairly constant in structure (apart from a cleft opening and closing; Holmes et al. 2004), but that the angle, which the lever arm made with the motor domain, could vary significantly. This immediately gave rise to the idea that the motor domain might bind to actin in a fairly well defined way, and that muscular movement could be associated with the lever arm swinging on the relatively fixed actin-attached motor domain, thus tending to make the actin and myosin filaments slide past each other.
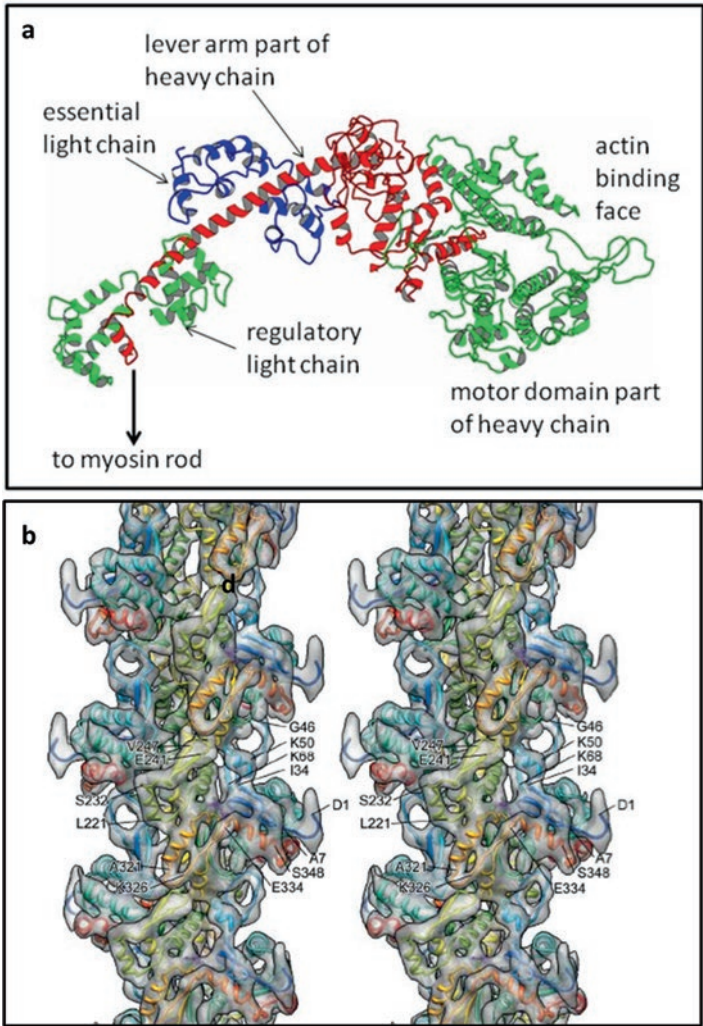
Fig. 11.6 (**a**) Structure of the S1 fragment of myosin (the myosin head) showing the heavy chain (*right green/red* part) and the α–helical region (*red*, *left*). The essential light chain is shown in *blue* and the regulatory light chain in *green* (*left*). (**b**) Good resolution (0.66 nm) structure of rabbit skeletal muscle F-actin as determined by Fujii et al. (2010; central part of their Fig. 11.2) using cryo-electron microscopy. Some amino acids are highlighted. ((**b**) Reproduced by permission Fujii et al. 2010)

11.2.4   Recent High Resolution Thin Filament Helical Reconstructions

The early helical reconstructions of actin alone or with tropomyosin/ troponin and heads bound were usually carried out on filaments that had been negatively stained for electron microscopy. However, the electron microscopy of frozen filaments,

228 although much more difficult, allows significantly higher resolutions to be achieved
229 (Xu et al. 1999). In addition, methods of analysis of electron microscope images of
230 helical filaments have been much improved (e.g. Egelman 2000). Here the helical
231 filaments can be divided up into short 'particles', which are analysed and averaged
232 in a procedure which optimises the estimated helical parameters. These are then
233 used in calculating the final reconstruction. The use of relatively short filament seg-
234 ments minimises the degradation of the reconstruction by deviations from pure heli-
235 cal symmetry that may occur along a long piece of filament (Li et al. 2011).
236   A relatively recent result from this approach applied to actin filaments is the
237 0.66 nm resolution structure determined by Fujii et al. (2010) and displayed in
238 Fig. 11.6b. Here the secondary structures in the actin molecules (α-helices, β-sheets,
239 loops etc) can be seen clearly. The known crystal structure of G-actin (Otterbein
240 et al. 2001; Protein Data Bank ID, 1J6Z) could be fitted readily into the density map
241 and it could then be refined using simulated annealing molecular dynamics with
242 stereochemical and non-bonded interaction terms restrained (Flex-EM; Topf et al.
243 2008). The new structure showed that interactions along the filament were relatively
244 strong, but that those between the two long-pitched strands of actin were compara-
245 tively loose. A more recent reconstruction of actin-tropomyosin at 0.37 nm resolu-
246 tion for F-actin and 0.65 nm resolution for tropomyosin has also been published
247 (von der Ecken et al. 2015).
248   Another significant advance was achieved when the structure of actin-
249 tropomyosin-myosin in the rigor state was determined using similar methods at
250 around 0.8 nm resolution (Behrmann et al. 2012). This structure (Fig. 11.7)
251 reveals interactions between a single myosin head and two successive actin mono-
252 mers along a long-pitched strand, together with one tropomyosin sub-repeat. As
253 expected the tropomyosin is positioned in the 'M' state, about 23° rotated about
254 the thin filament axis from the 'off' (closed or blocked; B) position. This was not
255 quite the 30° of Vibert et al. (1997), but was more rotated than their "C" state.
256 What is very apparent is that the rigor myosin heads and the tropomyosin strands
257 are tightly interacting.
258   One of the problems of the helical reconstruction approach applied to thin fila-
259 ments, when trying to probe the location of tropomyosin in different states, is that
260 troponin is still present (Vibert et al. 1997). Troponin is only on every seventh actin
261 monomer, so when helical averaging takes place the troponin density is smeared out
262 across seven actin monomers instead of one (as detailed by Squire and Morris
263 1998). Information about troponin is lost and the density that appears to be tropo-
264 myosin actually has troponin density added into it. Since the structure of troponin
265 presumably changes when it binds calcium, some of the observed apparent shift of
266 tropomyosin could be an artefact due to troponin movements and shape changes. In
267 short, another technique is needed to reveal troponin and to avoid the artefacts of
268 helical averaging. This is where true single particle analysis comes in.

Fig. 11.7 Good resolution (0.8 nm) structure of actin plus tropomyosin plus myosin subfragment 1 as determined by Behrmann et al. (2012). F-actin was prepared from rabbit skeletal muscle, and tropomyosin and myosin (MyoE) were purified from *Escherichia coli* (E. coli) and *Dictyostelium discoidium* cells respectively. Pseudo atomic models of the proteins have been fitted to the calculated density map (Reproduced by permission of Behrmann et al. 2012)
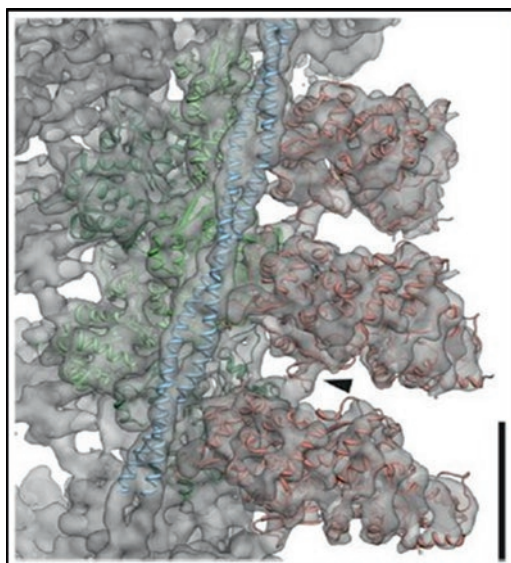
11.2.5 Finding Troponin – Single Particle Analysis

The method of single particle analysis was developed last century to generate 3D reconstructions of roughly spherical objects such as ribosomes and viruses (e.g. van Heel et al. 1996, 2000; Frank et al. 1996; Ludtke et al. 1999). The technique recognised that fields of globular particles lying on an electron microscope grid in negative stain, or preferably in a thin layer of ice, would probably lie in all orientations on the grid and would therefore provide multiple projected density views of the same object. As in tomography, the different views could then be recombined to produce a 3D model of the object. The viewing angle for each projection image (or class average formed from the average of many images corresponding to the same view) was then determined and the structure regenerated to give the required 3D density map. Spectacular results have been achieved for ribosomes and other protein complexes, exploiting recent developments in detector technology (Kuhlbrandt 2014).

Some while ago it was realised that even highly elongated particles, which show some form of axial periodicity, could be treated as single particles (e.g. AL-Khayat et al. 2004; Paul et al. 2004). In this case, images of long thin filaments could be chopped up into segments centred on the troponin density and each segment could then be treated as an image of a single particle. Different parts of the same filament or equivalent parts of different filaments would present different views of the same structure but rotated around the filament axis. Class averages could then be generated, the viewing angles found and reconstruction by back projection carried out.

This technique applied to thin filaments is significantly more difficult than helical reconstruction, mainly because each actin filament necessarily provides only
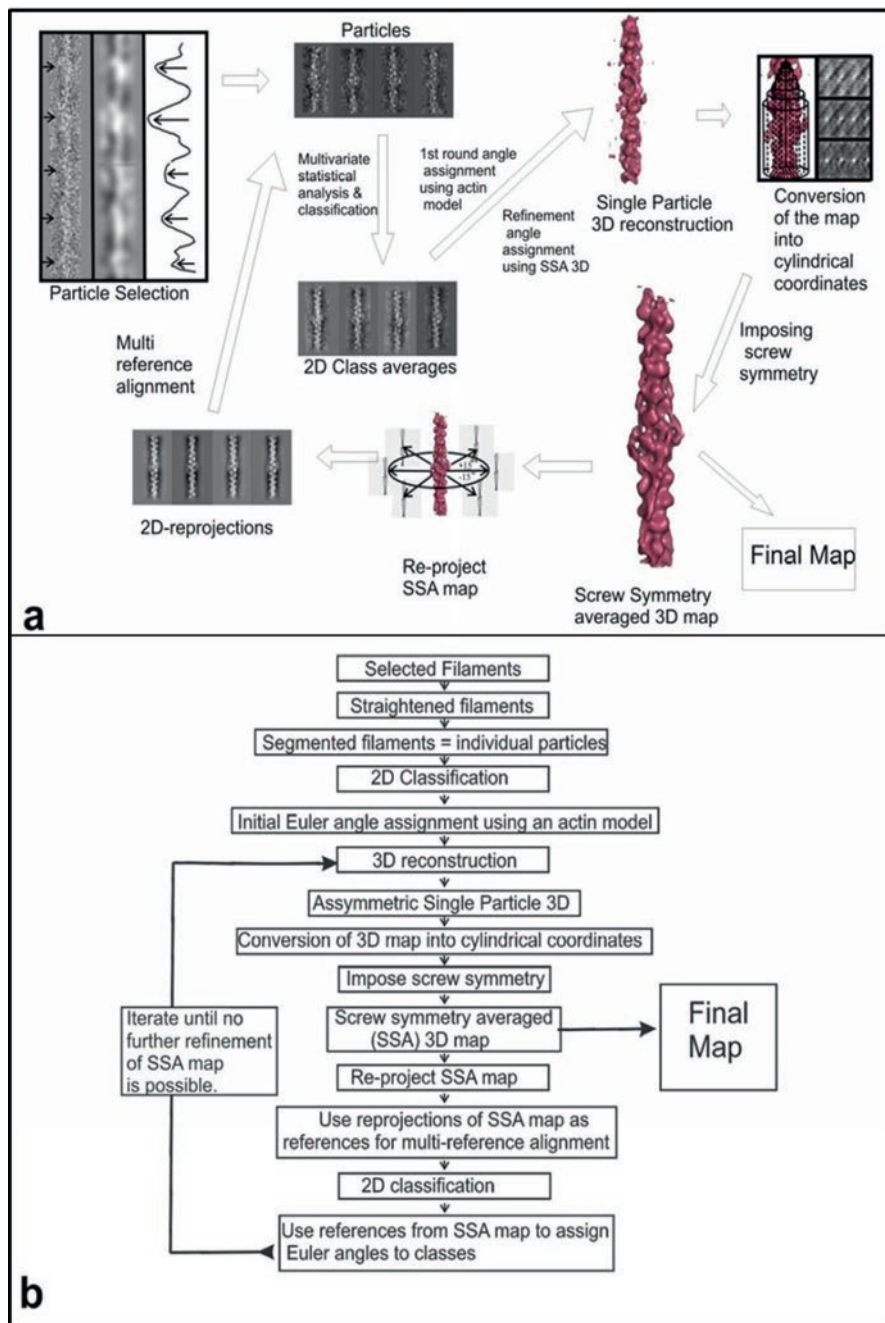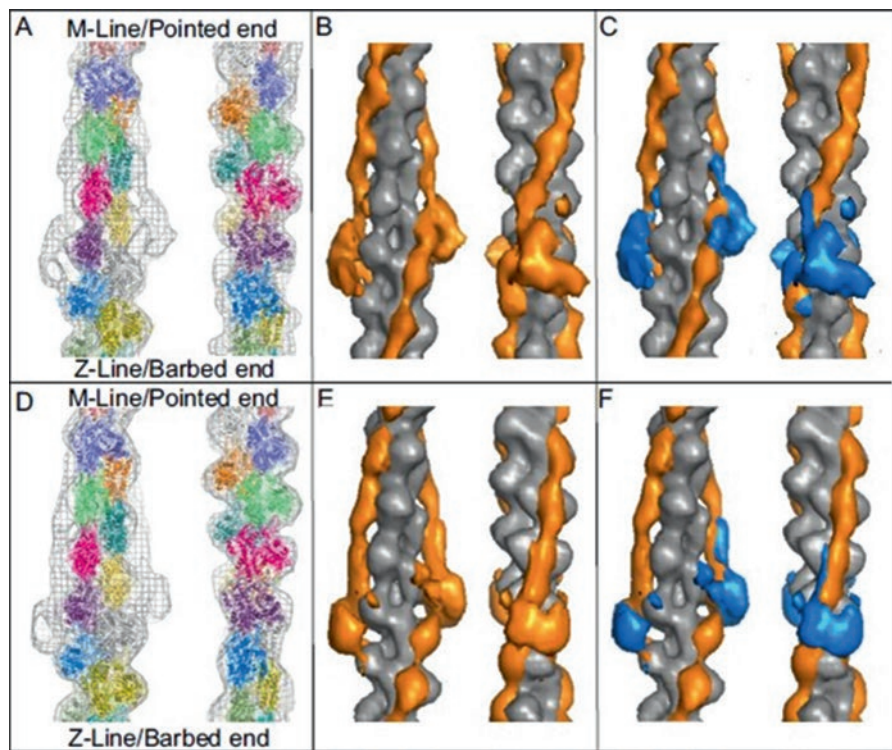
Fig. 11.8 Thin filament single particle image processing flow charts. (**a**) The cyclical nature of the image processing steps is depicted. Included here is an example of the particle selection procedure

one-seventh of the data that helical reconstruction has available. However, promis- 293
ing 3D reconstructions have already been obtained and the results are striking, even 294
though the work used negatively-stained filaments and the resolution achieved is as 295
yet only about 2.5 nm. The methods used are summarised in Fig. 11.8 (from Paul 296
et al. 2016). The most important step is to find the viewing angles of the different 297
images. What is usually done, is to compare the experimental images with projec- 298
tions of a reference structure seen at known viewing angles (projection matching). 299
In the case of the thin filament, this has been done in one case by using as a refer- 300
ence object a hypothetical model of actin / tropomyosin / troponin (Pirani et al. 301
2005). However, the result is a 3D reconstruction that is very similar to the original 302
reference structure with rather little extra density features, so it is likely that the 303
reconstruction was not refined away from the starting structure. A better approach, 304
when trying to discover the location of tropomyosin and the structure of troponin, is 305
to use only F-actin as the reference. In this case there can be no bias in what is found 306
out for tropomyosin and troponin, since they are not present in the reference struc- 307
ture. The results from this latter approach applied to thin filaments with and without 308
calcium bound (Paul et al. 2016) are shown in Figs. 11.9 and 11.10. The tropomyo- 309
sin in the 'off' state (low calcium; Fig. 11.9e, f) is in much the same position on all 310
seven actin monomers in the repeating unit, as in the case of the helical reconstruc- 311
tion. The troponin density wraps around the filament on one actin monomer and also 312
has a long tail of density, which extends along the filament (upwards in Fig. 11.9). 313
The structure of the whole of troponin is not known from X-ray crystallography, but 314
some parts of it have been solved including troponin-C plus parts of troponin I and 315
troponin-T (Takeda et al. 2003; Vinogradova et al. 2005). These incomplete struc- 316
tures can be fitted quite well into the density in the 3D reconstruction. The remain- 317
ing parts of troponin have been generated by using model building (Manning et al. 318
2011), and this arrangement, modified slightly, seems to fit quite well with what is 319
seen (Fig. 11.10). It is known that TnC, together with TnI and part of Tn-T (TnT2; 320
residues 159–259; Takeda et al. 2003; Vinogradova et al. 2005), form a globular 321
complex and that the rest of Tn-T (Tn-T1; residues 1–158) probably extends out 322

Fig. 11.8 (continued) where the filaments were visually inspected and the identification of tropo-
nin density was guided by the use of axial density profiles and the appearance of Fourier-filtered
images of the filaments in which the spatial frequencies ≤200Å and ≥500Å are suppressed. The
axial density profiles from these filtered images showed peaks originating from the troponin den-
sity. (**b**) A description of the image processing cycle used in the analysis of both the +Ca^{2+} and −
Ca^{2+} data. After segmenting the filament and generation of 2D class averages an actin model was
used to assign Euler (viewing) angles to create the initial single particle 3D reconstruction. This
asymmetric first 3D map was then converted into cylindrical coordinates and the screw symmetry
of the two actin strands was imposed. Re-projections of this screw symmetry averaged 3D map
were then used in a multi-reference alignment. The cycle of alignment, classification, 3D recon-
struction, imposing screw symmetry and re-projection was repeated until no further improvement
in the maps resolution was achieved. The final map was a screw symmetry-averaged single particle
reconstruction (Reproduced from Paul et al. (2016) Supplementary Information with permission)

Fig. 11.9 (**a–c**) Data from Ca^{2+}-treated filaments, (**d–f**) data from Ca^{2+}-free filaments. (**a**) and (**d**) Wire mesh representations of the single particle-based reconstructions of the thin filament in the two states. An atomic F-actin model is docked into the reconstruction and each subunit is colour coded. The barbed end (Z-band end) of the actin filament is at the bottom of the figure. (**b**) and (**e**) Difference density maps calculated by subtracting the docked F- actin model (*grey*) from the single particle reconstructions. This leaves the density attributable to the regulatory proteins troponin and tropomyosin (both *orange*). (**c** and **f**) Difference density maps calculated by subtracting docked F-actin (*grey*) and tropomyosin (*orange*) models from the single particle reconstructions leaving density attributable only to troponin (*blue*) (Reproduced from Paul et al. 2016 with permission)

323   from the globular region as long α–helical strands. It is likely that it is this elongated
324   part of Tn-T that accounts for the finger-like extension in the troponin density that
325   runs up the filament in Fig. 11.9c, f. One interesting feature of this is that the direc-
326   tion of the Tn-T tail is opposite to that reported earlier by Ohtsuki (1979). The Tn-T
327   tail really does appear to be directed towards the M-band or pointed end of the actin
328   filament, not the other way.
329   The results from the 3D reconstruction of the thin filament in the presence of
330   calcium are quite unexpected. It has been commonly assumed that tropomyosin
331   moves across the actin filament in much the same way on each actin, as in Fig. 11.3,
332   even though the tropomyosin sequence repeats are only quasi-equivalent. But the
333   actual structure is not like that. The tropomyosin repeats close to troponin on the
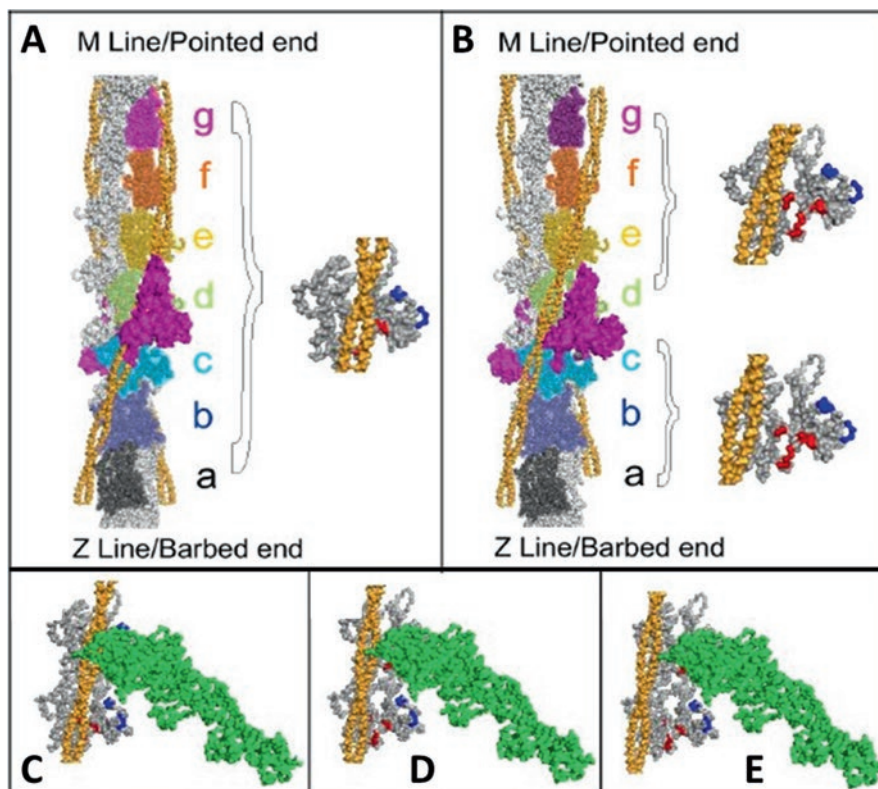
Fig. 11.10 Visualisation of the tropomyosin domain movements and myosin binding. (**a** and **c**) Structures of the Ca^{2+} -free state. (**b, d** and **e**) Structures of the Ca^{2+} -treated thin filament assembly. (**a**) and (**b**) The central region of the Ca^{2+} -free (**a**) and the Ca^{2+} -treated (**b**) reconstructions over a length of 14 actin subunits, two strands of tropomyosin (*orange*) and two troponin complexes. The core domains of the troponin are modelled using COMPHI, an atomistic model of cardiac troponin in the Ca^{2+}-treated state published by Manning et al. (2011). The model was generated using the existing crystal structure of the 52 kDa domain of human cardiac troponin in the Ca^{2+} -treated state (Takeda et al. 2003) together with missing regions that were constructed using secondary structure prediction. Subunits a to g of one strand of actin are colour coded and the second strand is *grey*. In the Ca^{2+}-free state (**a** and **c**) the position of tropomyosin is the same on every subunit and lies in the 'B' or blocked position where it would inhibit myosin binding. The position of tropomyosin is different on different subunits of the actin filament in the Ca^{2+} -treated state (**b**), where the average positions are illustrated (**a** and **b**; right inserts) for actin subunits d to g (closed state; set 1) and a to c (M-state; set 2). **c**, **d** and **e** show face on views of the actin subunits, with weak (*blue*) and strong (*red*) actin binding sites highlighted for the three distinct positions of tropomyosin. Subunits a, b and c show tropomyosin in the "M or Myosin state", subunits d, e, f, g show tropomyosin in a position more closely aligned to the "C or closed" state. In the Ca^{2+} -treated thin filament a myosin S1 head (*green*) can access all weak and potentially some strong binding sites on subunits e, f and g (**d**) and presumably all available binding sites on subunits a and b (**e**). An equivalent myosin head would be blocked on every subunit in the Ca^{2+} -free state (**c**) (Reproduced from Paul et al. 2016 with permission)

334 pointed end side shift across the filament by about 18° (tropomyosin repeats d to g
335 in Fig. 11.10b, which we refer to as set 1), but those on the other side of troponin
336 move on average by about 28° (tropomyosin repeats a to c to in Fig. 11.10b; set 2).
337 So, in the presence of calcium, set 1 tropomyosin are almost in the old closed state
338 of Vibert et al. (1997), but even in the absence of myosin, set 2 tropomyosin repeats
339 are in what is close to the 'M' state. Rather than tropomyosin moving as a fairly
340 rigid body, as part of a so-called Gestalt mechanism (Holmes and Lehman 2008),
341 the tropomyosin shift varies from actin to actin so that some myosin binding sites
342 are partially blocked and others appear to be completely open; the 'C' state of
343 Squire and Morris (1998) appears not to be an equilibrium between C and M states,
344 as in one of their original suggestions (Fig. 11.11a), but a defined mixture of 'C' and
345 'M' tropomyosin sub-repeats within the same tropomyosin molecule (Fig. 11.11b).

346 ## 11.2.6 *The Thin Filament Regulation Mechanism*

347 The new varying 'on' position for tropomyosin in the presence of calcium, suggests
348 a new scenario for thin filament activation in muscle. In the 'off' state the tropo-
349 myosin is presumably in a position where myosin head attachment is unlikely. But
350 it is as well to remember that none of these proteins will be static and the occasional
351 excursion of tropomyosin from its fully off position, which would allow occasional
352 head binding, would not be surprising. In the calcium-activated filament, which we
353 now know is a mixture of closed ('C') and myosin ('M') states, it is likely that
354 myosin heads opposite some points along actin (near tropomyosin set 2) will bind
355 more easily than those in other places (set 1) and limited contraction will proceed
356 (Fig. 11.11b). The more heads that then bind in strong states, the more the whole of
357 tropomyosin will be constrained to the 'M' state and eventually full activation will
358 occur (Fig. 11.11d).

359 ## 11.2.7 *Nebulin*

360 Chapter 10 in this volume discusses in detail another component of the thin fila-
361 ments in vertebrate striated muscles. This is the giant protein nebulin. It has a chain
362 weight of around 600–900 kDa and runs along the thin filaments in the I-band from
363 the Z-band to the actin filament tip (Fig. 11.12a). Nebulin has never been visualised
364 on the thin filament, but it is long enough to contribute a long mainly α–helical
365 strand along the filament, possibly running together with tropomyosin. There are
366 repeating units of about 35 residues which with a 0.15 nm subunit axial translation
367 in an α–helix gives an axial repeat of 5.25 nm, close to the actin monomer separa-
368 tion in a long-pitch actin strand of 5.5 nm. These repeats have been shown to bind
369 strongly to actin and they occur in groups of seven, corresponding to the length of
370 the regulatory unit in the thin filament. It is not known how many nebulin strands
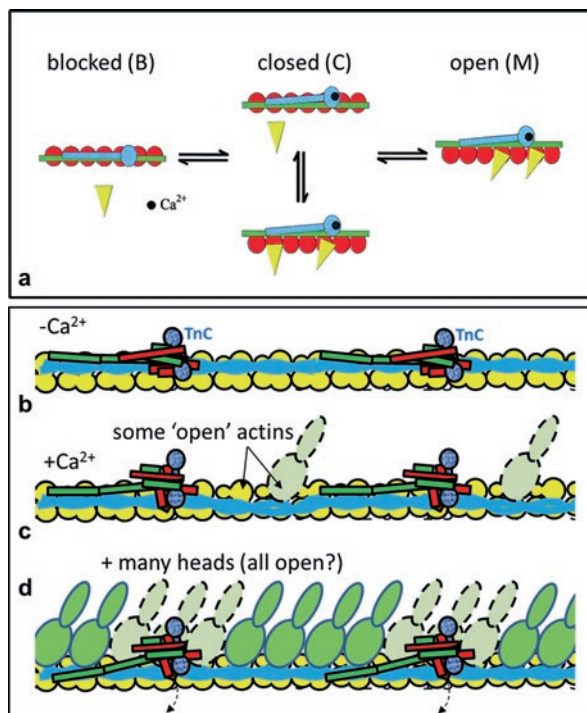
Fig. 11.11 (**a**) One of the possible mechanisms illustrated by Squire and Morris (1998) to explain the closed (**c**) state of thin filament regulation as being an equilibrium between the blocked and open states. (**b** to **d**) A novel mechanism of regulation unlike that in (**a**) where the 'C-state' is actually a mixture of the C and M states. Schematic diagrams of the thin filament assembly for simplicity are shown as a linear array (i.e. not helical). Protein components colour coded: actin (*yellow*), tropomyosin (*blue*) and troponin (TnC, speckled *blue*; TnI, *red*; TnT *green*). When the thin filament changes from the Ca^{2+} -free state (**b**) to the Ca^{2+}- bound state (**c**) the tropomyosin strands on the arrowed central actins (set 2) move further than those on actins adjacent to the Tn-T1 tail (*green*; set 1). Set 2 actins may be exposed enough for some myosin heads to bind (*dashed* outline). Bound heads going over to strong states may then activate the whole filament (**d**). The body of troponin may move out of the way (*dashed* arrows) to permit binding of further heads. (**b** and **c**) also illustrate a potential mechanism whereby the distal arm of TnT1 acting on the tropomyosin overlap region may swing to expose the binding sites on set 2 actins when Tn-C binds Ca^{2+} ((**a**) (Reproduced with permission from Squire and Morris (1998). (**b–d**) reproduced with permission from Paul et al. (2016))

there are per thin filament, but it is quite likely to be two. Nebulin occurs in many 371
splice isoforms of varying length and this length has been shown to determine the 372
length of the actin filaments in the I-band. The thin filament is terminated at the end 373
toward the M-band (the pointed end) by the protein tropomodulin (McElhinny et al. 374
2001). Other proteins associated with nebulin are desmin, titin and capZ (Fig. 11.12b) 375
as discussed in Chap. 10 of this volume. 376

Nebulin is not just a structural protein. It has been shown that its presence on the 377
thin filaments enhances the level of force produced by the sarcomere (Fig. 11.12c), 378
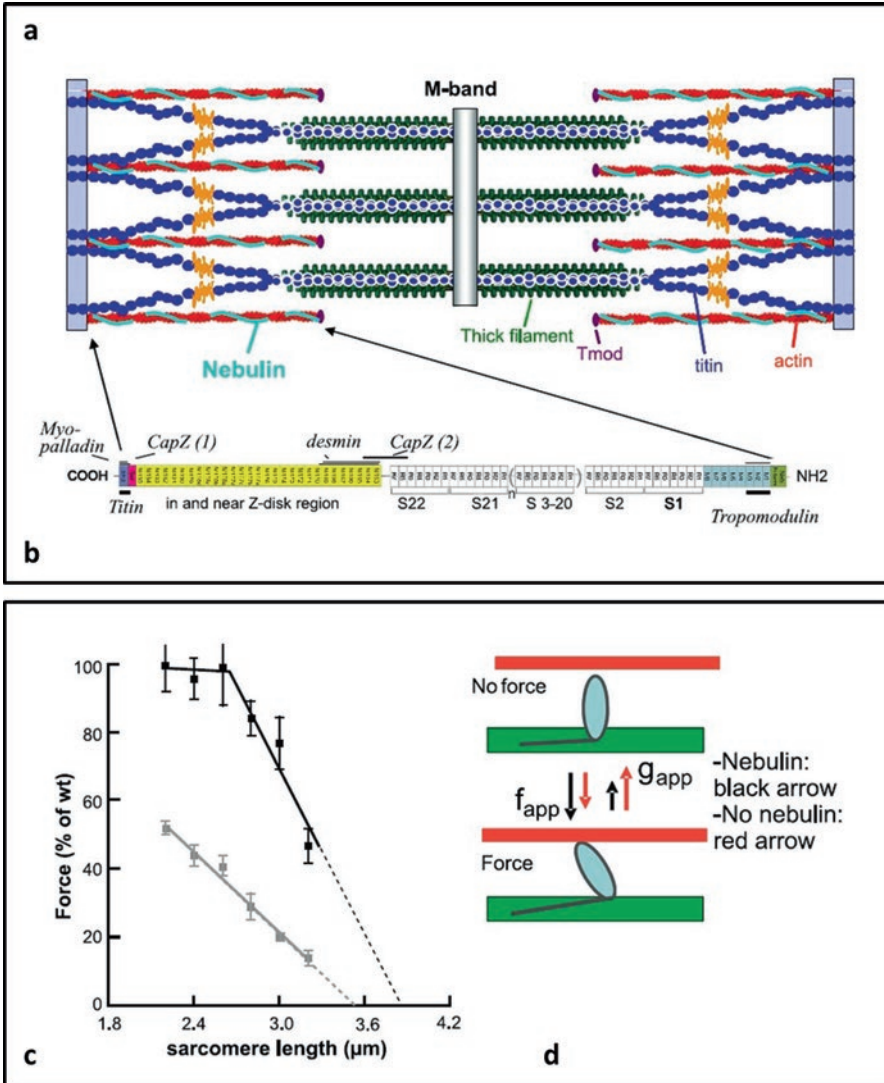
Fig. 11.12 Illustrations of the location and behaviour of nebulin on muscle thin filaments. (**a**) Layout of nebulin in the skeletal muscle sarcomere. Titin strands are also shown. (**b**) Modular organization of nebulin protein. Binding sites of nebulin-binding proteins are also shown: myopalladin, titin, the two reported capZ binding sites, CapZ(1) and CapZ(2), desmin and tropomodulin. (**c**) Comparison of the measured force sarcomere length relation of wild type and nebulin deficient NEB-KO muscle fibres. (**d**) Illustration of a 2-state crossbridge cycle and the effect of nebulin on the rate constant of transition from non-force-generating cross-bridges to force-generating cross-bridges f_{app} and on the reverse rate constant g_{app}. Nebulin increases f_{app} and slows $g_{app,}$ which has the net effect that the fraction of all available heads that generate force is increased (Reproduced from Labeit et al. 2011 with permission)

possibly changing the attachment and detachment rates of the myosin heads on   379
actin (f_{app} and g_{app}; Fig. 11.12d). Mutations of nebulin have also been shown to be   380
associated with various myopathies (e.g. Ottenheijm et al. 2013 and references   381
therein and Chap. 10).   382

The ease with which myosin heads can bind to actin also depends on where they   383
are coming from on the neighbouring myosin filaments. This is the topic of the rest   384
of this Chapter.   385

11.3   Myosin Filament Structure   386

11.3.1   Myosin Filament Symmetries   387

Vertebrate striated muscle myosin filaments are bipolar, with centrally packed anti-   388
parallel myosin molecules and outer parallel myosin molecules (Fig. 11.13a, b).   389
The filaments therefore have a central bare zone and outer regions where the myosin   390
heads project – the bridge regions (Fig. 11.13b). The first idea that the myosin heads   391
on myosin filaments might be relatively regularly organised on the myosin filament   392
surface came from the pioneering electron microscopy by Huxley (1963), and the   393
X-ray diffraction studies of frog muscle by Huxley and Brown (1967) and Elliott   394
(1964a; b, 1967). Huxley and Brown (1967) proposed that the myosin heads in frog   395
muscles were organised on 2-start helices with an axial shift between successive   396
subunits along the helices (the subunit axial translation) of 14.3 nm. The whole   397
structure would repeat after 43 nm. Shortly after this, in a pioneering study of the   398
appearances of longitudinal sections of insect flight muscle (IFM), Reedy (1968)   399
proposed that the IFM myosin filaments, with a bigger backbone diameter than   400
vertebrate filaments, were also on a 2-start helix with a subunit axial translation of   401
14.5 nm, but with a long repeat of 115 nm. In 1972, Small and Squire (1972) pub-   402
lished a structure for the face polar myosin ribbons seen in vertebrate smooth mus-   403
cle under some conditions (see Sect. 11.3.9), where the heads also had an axial shift   404
of 14.3 nm, but this time there was an apparent long repeat of around 72 nm.   405
Remembering that the myosin molecules making up these filaments were all rather   406
similar in structure (a long two-chain coiled-coil α–helical rod with two heads at   407
one end (Fig. 11.1a top), it seemed to Squire (1971, 1972) that such similar mole-   408
cules would not pack in such different ways. He suggested that vertebrate filaments   409
might have their heads on 3-start or 4–start helices and that IFM filaments might   410
have up to six coaxial helical strands. In this way the molecular packing of the myo-   411
sin rods in these different thick filaments would all be rather similar. In the end it   412
was found that vertebrate myosin filaments had their heads on 3-start helices (Squire   413
1972, 1973, 1981, 1986; Maw and Rowe 1980; Kensler and Stewart 1983) and IFM   414
filaments on 4-start helices (Wray 1979; Reedy et al. 1981; Morris et al. 1991).   415
Later work also showed that the heads on the filaments in scallop striated muscle   416
were on 7-start helical strands (Millman and Bennett 1976; Vibert and Craig 1983;   417
Craig et al. 1991; Vibert 1992; AL-Khayat et al. 2009a, b; Woodhead et al. 2013).   418
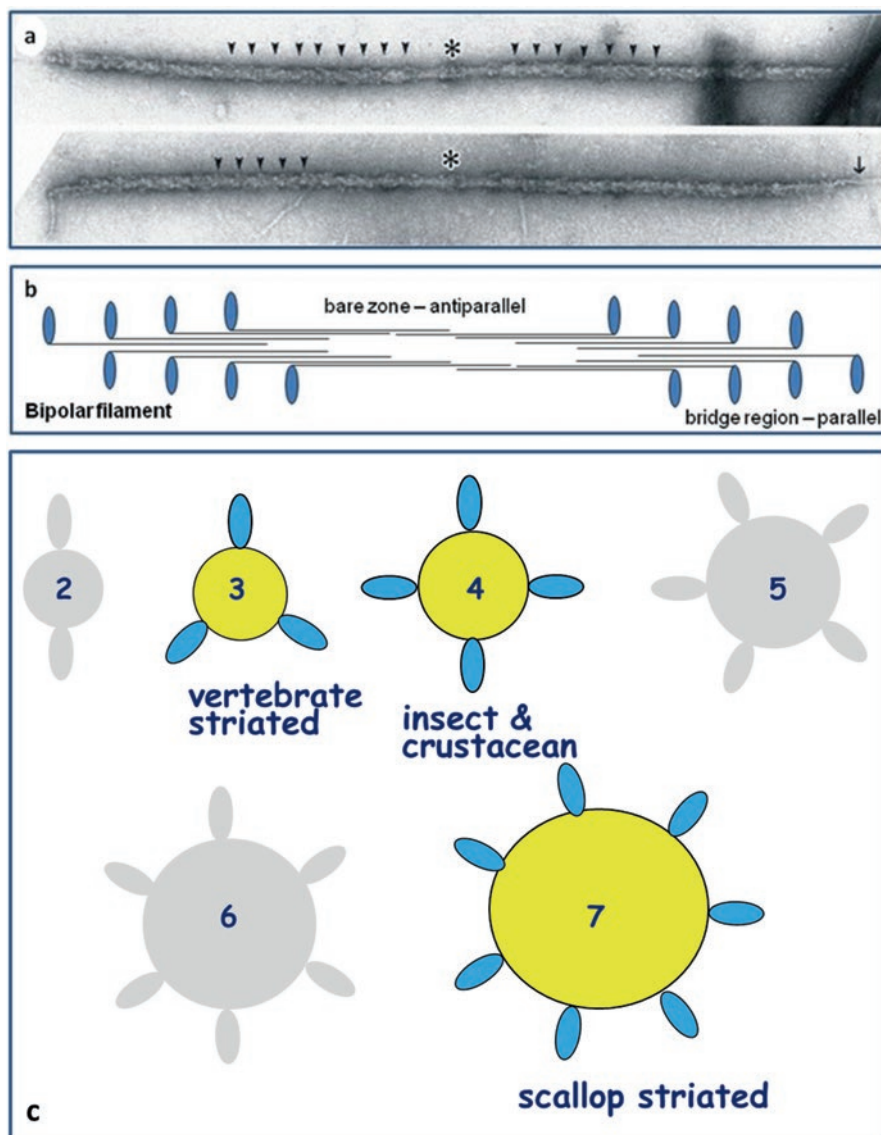
Fig. 11.13 (**a**) Electron micrograph of isolated bipolar thick filaments from fish muscle showing the axial repeat patterns on each side of the central M-band region (starred). (**b**) Schematic diagram to show the antiparallel arrangement of myosin molecules in the bare zone of striated muscle thick filaments and the parallel packing in the filament bridge regions. The bridge regions are very much longer in real filaments. (**c**) Illustration of the possible rotational symmetries that myosin filaments might possess. Those filaments identified so far are the 3-start, 4-start and 7-start helices. 2-start filaments are probably physically impossible, but it is conceivable that 5-start or 6-start filaments might be found

All these structures are illustrated in Fig. 11.14, where it can be seen that the axial and lateral separation of the myosin heads on the filament surfaces are all rather similar. Figure 11.15 compares the low-angle X-ray diffraction patterns from fish muscle (a) and insect flight muscle (b), both of which show superb 3D order, similar meridional peaks at around 14.3–14.5 nm, but different layer line spacings revealing the different myosin head lattice geometries.

AU2

Hanson and Lowy (1963), Szent-Gyorgyi et al. (1971) and Hardwicke and Hanson (1971) showed that the very large myosin-containing filaments in molluscan smooth muscles have a thin surface layer of myosin on a core of paramyosin. Paramyosin molecules are rather like the rod part of myosin without the heads at one end. Squire (1971) showed that the amounts of myosin and paramyosin in muscles with different filament diameters were consistent with the myosin packing into similar 2D nets of heads to those in Fig. 11.14a–d, with a central core of paramyosin molecules. The structures of these paramyosin filaments will be discussed later in the Chapter (Sect. 11.3.8).

Figures 11.13c and 11.14a–d show that the known myosin filaments form a family with different rotational symmetries – 3-start (vertebrate), 4-start (IFM, *Limulus*, crab etc) and 7-start (scallop). Apart from very large paramyosin filaments, are these the only possibilities? For example, could there be 5-start and 6-start filaments in some muscles, probably invertebrate, that have not yet been discovered (Fig. 11.13c)? In a detailed analysis of the X-ray diffraction patterns from some crustacean muscles, Wray (1979) suggested that myosin filaments in lobster abdominal flexor muscle might be 4-stranded, whereas those from the lobster crusher claw muscle might be 5-stranded, but this has yet to be confirmed.

11.3.2 Myosin Head Organisation

With many myosin filament lattice symmetries known, the next question to ask is how are the myosin heads arranged on these surface lattices? Fig. 11.14e–g illustrate schematically the regular ways in which myosin heads might conceivably be organised if the heads are stabilised by interaction with other heads. Each layer of heads spaced by 14.3–14.5 nm is usually known as a 'crown' of heads. The two heads of a single molecule might interact with each other and might point up the same long period helices as in the type 1 configuration (Fig. 11.14e). Alternatively they might interact across the filament with heads from adjacent molecules in the same crown (type 2; Fig. 11.14f) or they might interact with heads from other molecules in successive crowns along the filament (type 3; Fig. 11.14g). Early analysis of X-ray diffraction data suggested that the elongated heads in vertebrate striated muscles might be tilted up the filament, perhaps along the long period helices as in the type 1 structure, to explain why the 1st and 2nd (42.9 and 21.5 nm) layer lines in X-ray diffraction patterns (Fig. 11.15a) were relatively strong compared with the meridional M3 reflection at 14.3 nm (Squire 1975). The structures of isolated myosin filaments (e.g. Fig. 11.13a) were then studied using electron microscopy and
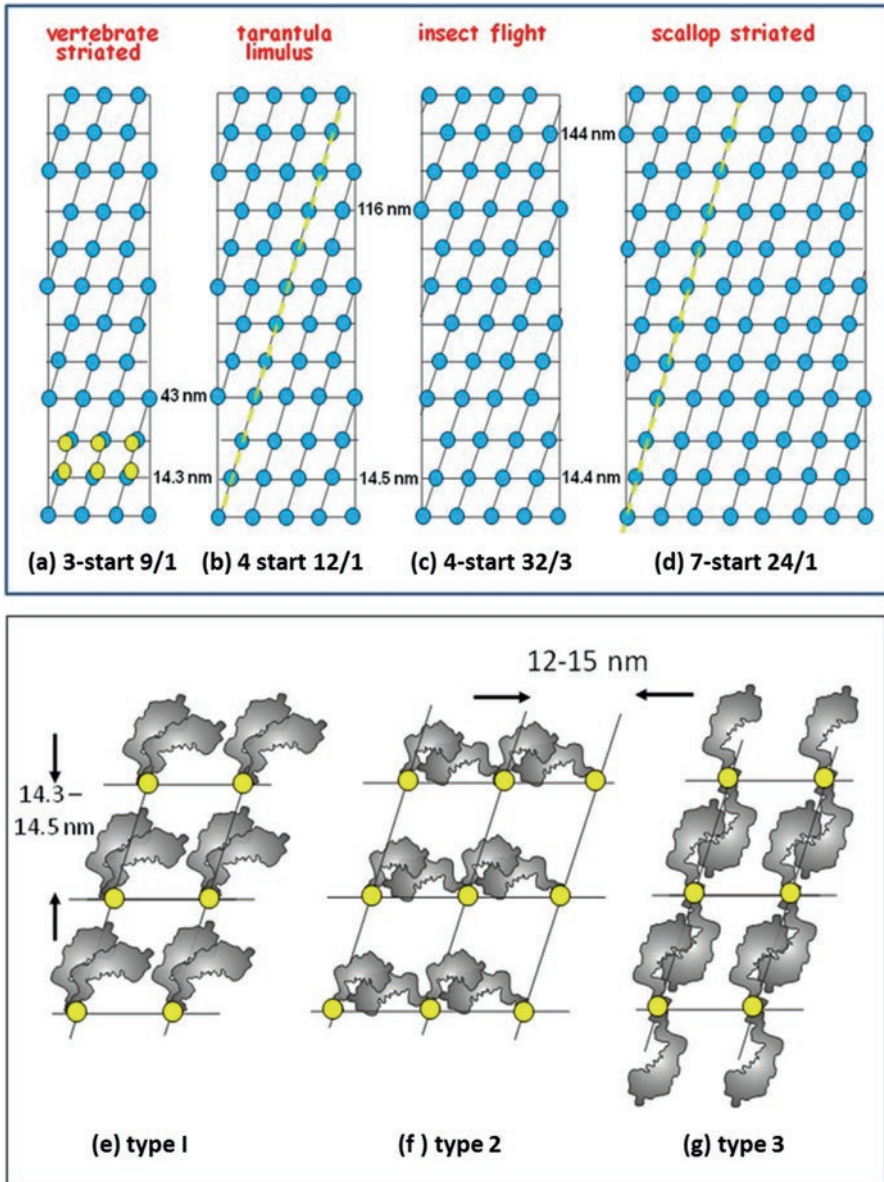
Fig. 11.14 (**a–d**) The known myosin head surface lattices of a variety of myosin filaments as labelled. The 14.3–14.5 nm crown repeat is a characteristic of all myosin filaments, but the angle that the long period strands follow (e.g. the *yellow dashed lines* in (**b**)) varies slightly to give the filaments different axial repeats. All vertebrate striated muscle bipolar filaments are 1.57 μm long, have threefold symmetry and have an axial repeat after three crowns of 43 nm. 4-start filaments can have either a 43 nm axial repeat (e.g. (**b**) tarantula, limulus) or a 115 nm repeat (c: insect flight muscle). Scallop thick filaments are the only known 7-start filaments. Their axial repeat is 144 nm. Note that the crowns in vertebrate striated muscles are not equivalent; there are small axial and
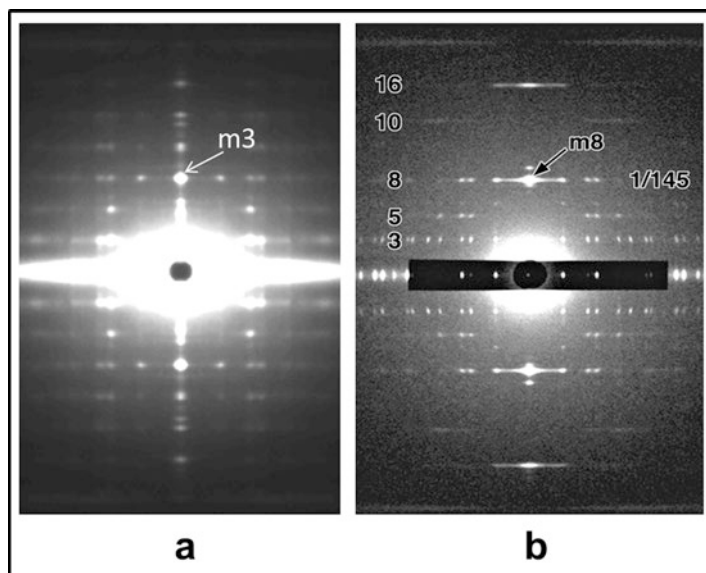
Fig. 11.15 Low-angle X-ray diffraction patterns from striated muscles held vertical. (**a**) The pattern from bony fish muscle and (**b**) the pattern from insect flight muscle. The meridional reflection from the crown spacing is m3 in (**a**), the 3rd order of the 43 nm repeat, and m8 in (**b**), the 8th order of the 115 nm repeat. These two muscle types are the only striated muscles known to have good 3D order as exemplified by the sampling of the (horizontal) layer lines by (vertical) row lines, giving well defined diffraction spots ((**a**) from the work of Harford and Squire 1986; (**b**) courtesy of Professor M.K. Reedy)

helical reconstruction methods (e.g. Stewart and Kensler 1986; Crowther et al. 1985; Offer et al. 2000 and many more). Filaments from most sources tended to show ridges of density along the long period helices in one of the nets in Fig. 11.14, and these were all interpreted as myosin heads in the type 3 conformation (Fig. 11.14g). Examples of some excellent reconstructions from scorpion and *Limulus* muscles (Stewart et al. 1985) are shown in Fig. 11.16, where it appeared that type 3 interactions might well occur. The problem with this and other similar studies was that the resolution involved was simply not quite good enough to be able to distinguish the alternative head configurations.

460
461
462
463
464
465
466
467
468

Fig. 11.14 (continued) azimuthal perturbations of the head arrays, as shown by the *yellow dots*. (**e** to **f**) Schematic illustrations of the kinds of head arrays that might occur in resting muscle myosin filaments if their organization is stabilised by head-to-head interactions. (**e**) Type 1 has heads in the same myosin molecule interacting. (**f**) Type 2 has heads from adjacent myosin molecules in a crown interacting. (**g**) Type 3 has heads from successive crowns interacting. For many years it was thought that the head arrangement in (**g**) occurred on many filament types, but this was based on 3D reconstructions where the resolution was not sufficient to distinguish between the alternatives. It is now known that type 1 interactions occur in all muscle myosin filaments so far studied in detail, apart from those in insect flight muscle where Type 2 interactions seem more likely (Adapted from Squire et al. 2005)
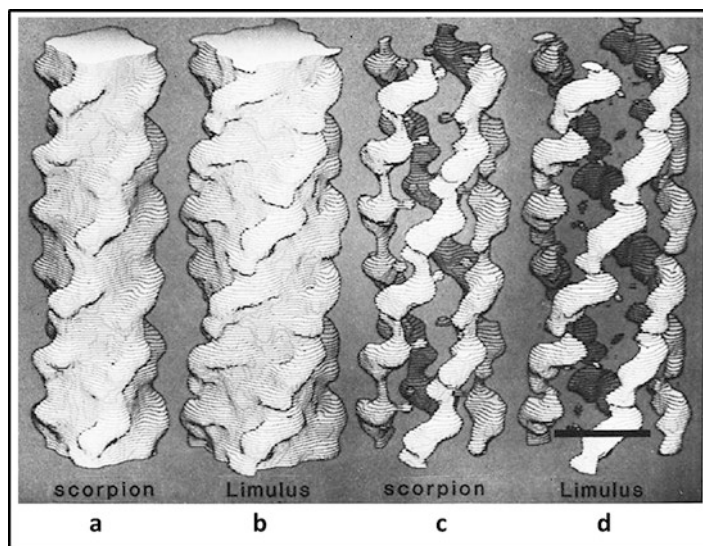
Fig. 11.16 Early 3D reconstructions of arthropod muscle thick filaments (**a**) and (**c**) scorpion; (**b**) and (**d**) *Limulus*. The reconstructions were obtained from negatively stained filaments and the helical reconstruction method (DeRosier and Moore 1971) at about 5 nm resolution. They show apparent axial spreading of head density along the long period helical tracks of the cross-bridge lattice (see Fig. 11.14b) (Reproduced from Stewart et al. 1985 with permission)

As in the case of actin filaments, the real breakthrough came when single particle methods were applied to these filaments (AL-Khayat et al. 2004). The first results from this were from the 4-start myosin filaments in tarantula muscle. These filaments have the advantage that the myosin heads appear to be organised on perfectly regular helices, so helical averaging could be applied. Tarantula filament images obtained from frozen-hydrated specimens were studied using single particle analysis and the Egelman (2000) helical averaging procedure, and the study of myosin filaments took a huge step forward (Fig. 11.17b; Woodhead et al. 2005). Here it was found that tarantula myosin heads, previously thought to be in the type 3 conformation, were actually in the type 1 conformation, with the two heads in one myosin molecule interacting with each other, but in slightly different conformations (Figs. 11.17a and 11.18). In a previous study of a 2D raft of myosin heads from vertebrate smooth muscle viewed in ice, Wendt et al. (2001) had seen a similar two-headed interaction with the motor domain of one head interacting with the converter domain of the other head. Smooth muscle myosin is regulated by phosphorylation of the regulatory light chain and this smooth muscle myosin conformation was that found in the absence of phosphorylation. These authors described a free head and a blocked head, but the conformation could be such that neither head can bind to actin. The fact that this same conformation with free and blocked heads (Fig. 11.18) appeared on the surface of tarantula myosin filaments gave the hint that this might be a general theme, at least for myosin-regulated muscles (Craig and Woodhead
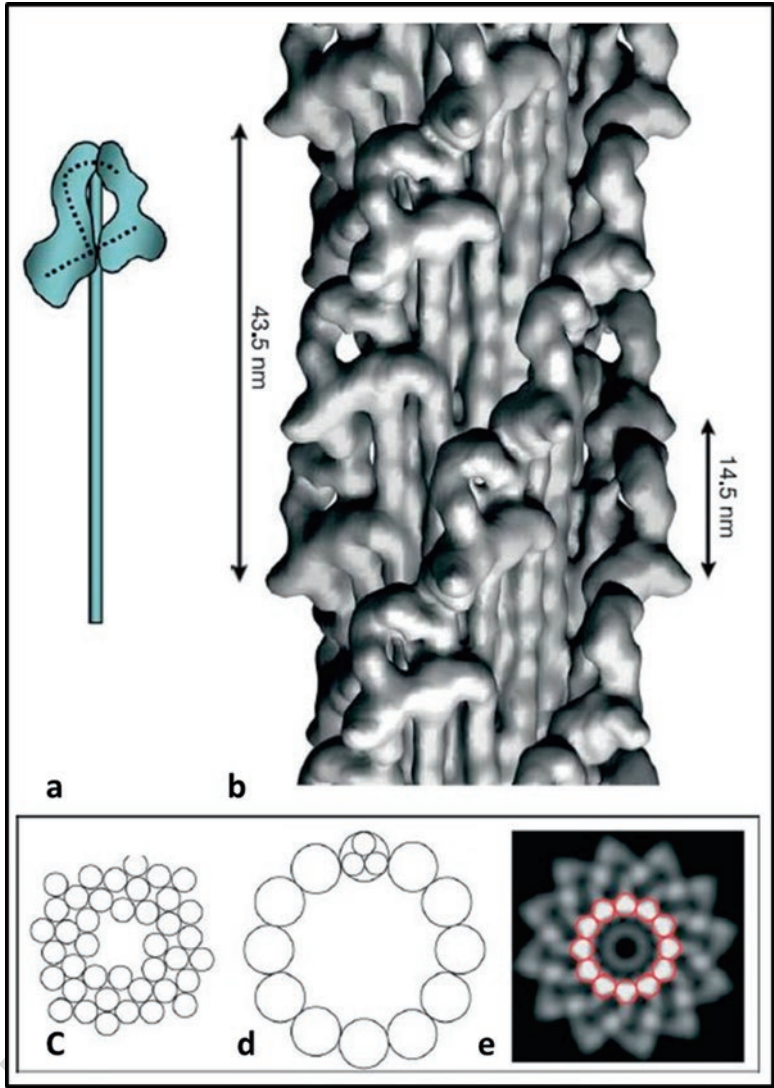
Fig. 11.17 (**b**) Surface view of a 3D reconstruction of tarantula muscle myosin filaments (bare zone at the *bottom*) by single particle analysis showing the interacting head motif illustrated schematically in (**a**) (Adapted and reoriented from Woodhead et al. (2005) to be consistent with other figures in the Chapter) (**c–e**) Possible models (**c, d**) and the average projection (**e**) of the cross-section ((**a**) and (**b**) Adapted from Woodhead et al. 2005; (**c–e**) from Craig and Woodhead 2006)

2006; Alamo et al. 2008). This idea was extended when the structures of the 4-start filaments in *Limulus* and the 7-start filaments in scallop striated muscle were studied by single particle analysis (Zhao et al. 2009; AL-Khayat et al. 2009a, b; Woodhead et al. 2013).

Fig. 11.18 Details of the interacting head motif in Fig. 11.17a, b with the atomic model of vertebrate smooth muscle heavy meromyosin (PDB 1i84; Wendt et al. 2001) fitted to the density in the reconstruction of tarantula thick filaments (bare zone to the bottom). Best fit of the crystal structure shown in (**b**) and the ribbon diagram without the density map shown in (**a**), where particular features of the heads are labelled (*MD* motor domains, *ELC* essential light chains, *RLC* regulatory light chains) (Modified and reoriented from Woodhead et al. (2005) to be consistent with other figures in the Chapter)
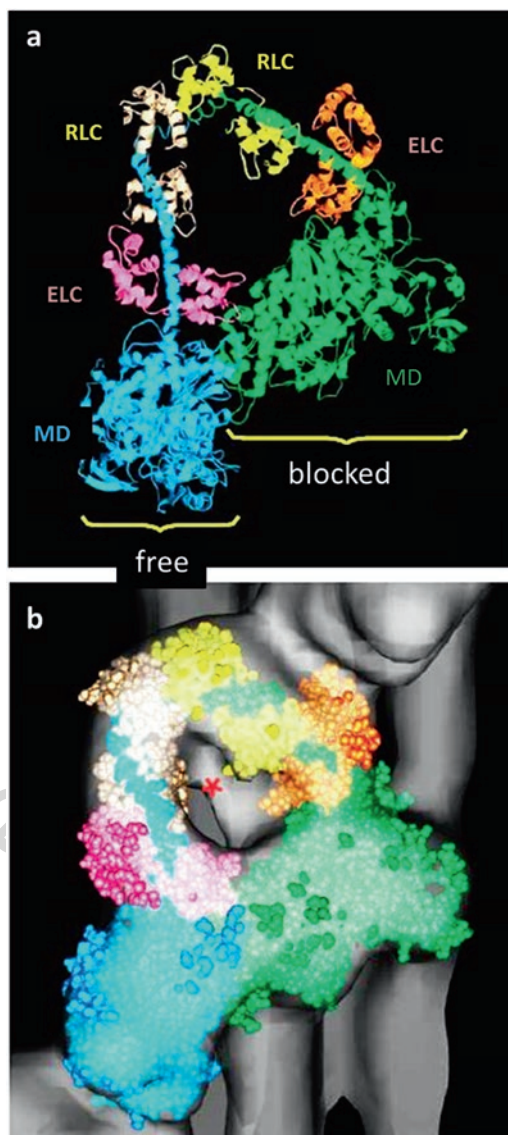
More surprising results came from similar analysis of vertebrate striated muscle myosin filaments, which are thin filament-regulated (e.g. AL-Khayat et al. 2006). What has not been described yet is the fact that the crowns in these vertebrate filaments are not all the same; there are systematic perturbations of the myosin heads away from strictly helical symmetry. Indications of axial and azimuthal head shifts are shown in Fig. 11.14a. There is still approximately a true repeat after three crowns or 42.9 nm, but the three crowns in this repeat are different. The axial perturbations

were first shown by Huxley and Brown (1967) for frog muscle and by Harford and Squire (1986) for fish muscle looking at the meridian of the X-ray diffraction patterns, but they may also involve azimuthal displacements around the filament axis. This means that the helical-averaging single particle approach of Egelman (2000) is not applicable and, as in the case of the thin filament (Paul et al. 2004), to see the structure properly requires full single particle analysis without helical averaging (AL-Khayat et al. 2004).

11.3.3 Myosin Filaments in Vertebrate Striated Muscles: MyBP-C and Titin

Vertebrate striated muscle myosin filaments are bipolar with a bare zone half way along their length where there is antiparallel packing of myosin molecules (Figs. 11.1a and 11.13a, b). The myosin heads then appear in the two outer parts of the filaments, conveniently termed the bridge regions (shown schematically in Fig. 11.13b). However, even though there is a dominant 42.9 nm axial repeat, the bridge regions are not constant in structure, as a purely helical filament would be. As described in Chap. 10 (Trinick and Tskhovrebova 2016; see also Granzier and Labeit, 2005, 2007), the giant molecule titin runs along the myosin filament from the M-band to the filament tip, where it forms so-called end-filaments (Trinick 1981), and then it continues through the I-band to the Z-line. The myosin filament part of titin, mostly composed of immunoglobulin (Ig) and fibronectin (Fn3)-like domains, has systematic pseudo-repeats along it as in Fig. 11.19a.

In the centre of each bridge region is a part of the filament where the extra protein C-protein (or myosin binding protein C; MyBP-C; Offer et al. 1973; Bennett et al. 1986) is located. This region, the C-zone (Sjostrom and Squire 1977), coincides with part of the titin sequence where there are repeats of sets of 11 domains. Successive domains are separated axially by about 3.9 nm on average, giving a repeat after 11 domains of 42.9 nm – exactly the same as the myosin axial repeat. MyBP-C in vertebrate skeletal muscle consists of 10 domains which, like much of titin, are Ig-like or Fn3-like (Fig. 11.19b). Originally, it was thought to be just a myosin-binding protein with domains C8 to C10 binding to myosin and to titin on the myosin filament. But more recently it has been found that the outer end of C-protein, around domains C1 and C2 in vertebrate skeletal muscle, binds to actin filaments (Squire et al. 2003; Whitten et al. 2008; Luther et al. 2011). The C-protein therefore acts as a bridge between the myosin and actin filaments, at least under some conditions (Fig. 11.19c; Luther and Craig 2011). Cardiac muscle MyBP-C has an extra domain (C0) at its N-terminus (Fig. 11.19b) and both skeletal and cardiac MyBP-C have a Pro-Ala-rich linker on the N-terminal side of C1, all of which may also be involved in actin binding (Squire et al. 2003). Another myosin-associated protein is H-protein (MyBP-H; Fig. 11.19b) which is also a molecule with Ig and Fn3-like domains; it is found closer to the bare zone than MyBP-C (Bennett et al. 1986). Other related proteins which cross-link myosin filaments in

Fig. 11.19 (**a**) The A-band part of titin consists of a repeating pattern of 11 Ig and Fn3 domains grouped in 11 copies from C-terminus to N-terminus as (Fn-Fn-Fn-Ig-Fn-Fn-Fn-Ig-Fn-Fn-Ig) starting at the edge of the bare zone. It then continues as six copies of the repeat (Fn-Fn-Fn-Ig-Fn-Fn-Ig) plus a few extra domains out to the myosin filament tip. (**b**) C-protein (MyBP-C) in cardiac and skeletal muscle. The common features are ten domains, which are Fn3-like, and Ig-like, num-bered C1 to C10. The C-terminal domains C8, C9, C10 are associated with myosin and titin binding. Between C1 and C2 is a sequence which binds to myosin S2. Cardiac C-protein has an

the M-band are myomesin and M-protein (Agarkova and Perriard 2005; Tskhovrebova and Trinick 2012; Fig. 11.19b).

For some years there was uncertainty about whether MyBP-C might have a different axial repeat from myosin, because various features of the meridional X-ray diffraction pattern (Rome et al. 1973) and analysis of longitudinal sections of vertebrate muscle A-bands (Squire et al. 1982) suggested that MyBP-C might have an axial repeat around 44 nm rather than 42.9 nm. It was then found that the longer repeat, which certainly did come from MyBP-C, was not the myosin repeat, but was due to the axial disposition of the actin ends of the MyBP-C molecules, while the myosin ends of MyBP-C were still on a 42.9 nm repeat (Squire et al. 2003). Interestingly, if the length of the C-zone was much more than seven to nine 42.9 nm repeats, then this apparent longer spacing for the actin-binding ends would have disappeared and reverted to 42.9 nm. The fact that MyBP-C can bind to actin under certain conditions leads one to wonder whether it has some sort of regulatory role in the contractile cycle, and this has led to much further work and discussion (Kunst et al. 2000; Kulikovskaya et al. 2003; Winegrad 2003; Luther et al. 2008; Ababou et al. 2008; Kensler and Harris 2008; Govada et al. 2008; Shaffer et al. 2009; Luther et al. 2011; Craig et al. 2014; Walcott et al. 2015; van Dijk et al. 2015; Previs et al. 2015; Moss et al. 2015; Kampourakis et al. 2015 and many others).

11.3.4 *Myosin Filaments in Vertebrate Striated Muscles: The Myosin Head Array*

The presence of MyBP-C in the C-zone and the fact that titin has a C-zone-specific sequence might suggest that the myosin head configurations in the C-zone are different from those in the other parts of the bridge region; the P-zone (P for proximal; between the bare zone and the C-zone) and the D-zone (D for distal; outside the C-zone) (Sjostrom and Squire 1977). Indeed, recent evidence from probe studies suggests that this is so (Fusi et al. 2015). A great deal of analysis of the low-angle X-ray diffraction data from the myosin filaments, particularly in fish muscles, where the A-band is highly ordered, was rigorous, but it was all based on the assumption that the myosin head organisation is the same along all of the vertebrate striated muscle bridge region (Fig. 11.15a); Harford and Squire 1986; Hudson et al. 1997; AL-Khayat and Squire 2006). On this assumption, the number of X-ray

Fig. 11.19 (continued) additional Ig domain (C0) at its N-terminus. Phosphorylation sites are indicated by a rectangle in the S2 binding site and in C5. A pro-Ala-rich domain is present at the N-terminus in both isoforms; it links C0 and C1 in the cardiac molecule. (**c**) Illustration of the cross-linking of the myosin and actin filaments by C-protein (MtBP-C) and possible interaction of 'sentinel' myosin heads (SH) with actin in relaxed muscle. *A* actin, *Tn* troponin, *Tm* tropomyosin, *MD* myosin motor domain, *RLC* regulatory light chain, *LA* lever arm, *IHM* interacting heads motif (cf Fig. 11.15), MyBP-C myosin binding protein C (C-protein) (Reproduced from Woodhead and Craig 2015)

574 observations on the myosin layer lines out to a resolution of around 6 nm was greater
575 than the number of parameters to fit in a model and unique solutions could be
576 obtained. But X-ray diffraction provides information about average structures, so if
577 the myosin head organisation varies along the vertebrate myosin filament then this
578 poses a real problem for X-ray diffraction analysis. To model the P-zone, C-zone
579 and D-zone heads as different structures would require more parameters than there
580 are X-ray observations. Only if there was good information from another source
581 would the analysis of vertebrate X-ray diffraction patterns be fully tractable.

582 As mentioned above, the way around this problem and around the fact that the
583 filaments are not helical is to use single particle analysis without helical averaging.
584 This was been done successfully for rabbit cardiac myosin filaments in negative
585 stain (Zoghbi et al. 2008; AL-Khayat et al. 2008). An improved structure was then
586 obtained by AL-Khayat et al. (2013) using just the C-zones in myosin filaments
587 from the ideal source, the human heart, once again in negative stain. A particle was
588 taken to be approximately two 42.9 nm repeats, with one of the MyBP-C stripes as
589 the centre point (Fig. 11.20b). We know that these filaments have threefold rotational
590 symmetry (Fig. 11.14a), so this could be used to help get a starting model from one
591 of the class averages. An independent, reference-free, angular assignment method
592 was also used (Padwardhan et al. 2004). The result is shown in Fig. 11.21a.

593 What is striking from this analysis and that of Zoghbi et al. (2008) is that the
594 head pairs are in very similar arrangements to the head pairs on the tarantula and
595 scallop thick filaments discussed earlier. Even though in vertebrate filaments the
596 three crowns of heads are different (Fig. 11.21b), they are all in similar conforma-
597 tions; it is the angle of the whole head pair assembly that changes in the different
598 crowns. Note that the views of the head pairs in Fig. 11.21b are from the inside of
599 the filament where the end of the myosin rod can be seen inserting into the heads,
600 whereas those in Fig. 11.18 are from the outside. There are still free heads and
601 blocked heads, as in smooth muscle myosin (Wendt et al. 2001), but this time the
602 myosin filaments are not directly myosin-regulated. The vertebrate striated muscle
603 essential light chain can be phosphorylated reversibly during contraction, but this
604 seems to be a modulating process rather than the fundamental regulatory switch. So
605 the head pair arrangement appears to be a common theme in most types of myosin
606 filament. The only known exception to this is the thick filament of insect flight
607 muscle, which is discussed in the next section.

608 Figure 11.21a showing the human cardiac myosin filament also reveals densities
609 which were interpreted as being due to titin and to MyBP-C. Each half myosin fila-
610 ment is thought to be associated with six titin strands (Liversage et al. 2001; Knupp
611 et al. 2002) and it is likely that these occur in three pairs. The density in the 3D
612 reconstruction appears to be able to accommodate such titin pairs and the 3.9 nm
613 axial repeat is also evident, tending to confirm the density as being due to titin. At
614 the top end of the Figure there is also enough extra density to account for domains
615 C8 to C10 of MyBP-C, also with a 3.9 nm axial repeat, so we have a general picture
616 of the head, titin and MyBP-C organisation in these cardiac thick filaments.
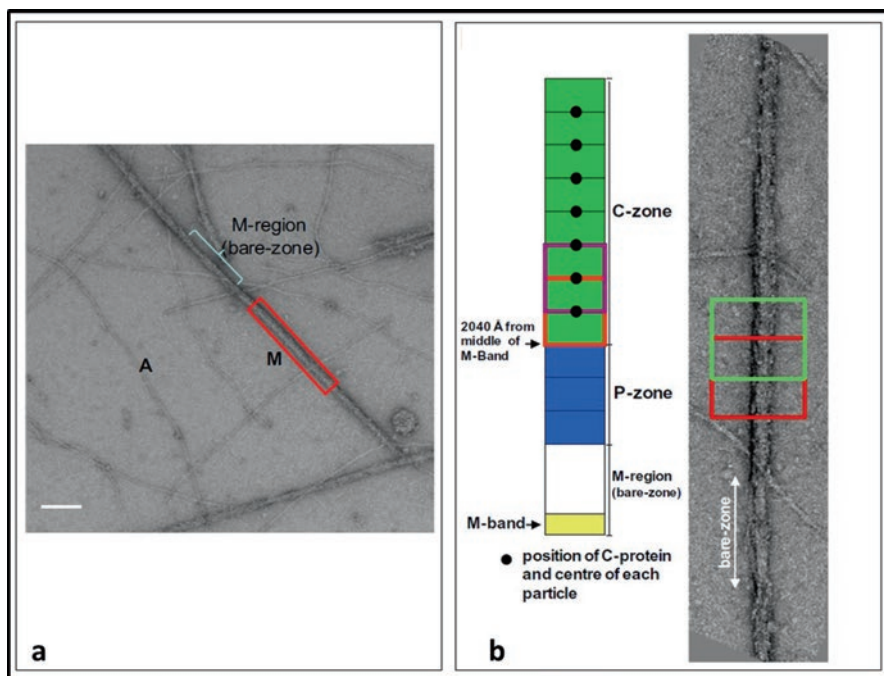
Fig. 11.20 (**a**) Electron micrograph of isolated myosin filaments (M) from the ventricular muscle of normal (undiseased) human heart in the relaxed state. Some actin filaments (A) can be seen in the background. Scale bar 200 nm. (**b**) left schematic diagram showing the different A-band regions within a half filament from the M-band at the bottom, the M-region, the P-zone and the C-zone (Sjostrom and Squire 1977). For the 3D reconstruction in Fig. 11.21 particles were selected from the C-zone only and the particles were about two C-repeats long (about 89 nm; *rectangular boxes* in (**b**)), but centred on each C-repeat (Reproduced from Al-Khayat et al. (2013) Supporting information with permission)

11.3.5   *Myosin Filaments in Insect Flight Muscle*   617

As in many aspects of its structure and contractile behaviour, when it comes to the   618
myosin filaments in insect flight muscle they are in a class of their own. After the   619
brilliant pioneering work of Reedy (1968) and that reported in his subsequent   620
papers, it was found that the IFM myosin filaments have their heads on 4-start heli-   621
ces with a crown separation of 14.4 nm and a filament repeat after 115 nm   622
(Fig. 11.14c). An early helical reconstruction of isolated IFM filaments showed this   623
4-strandedness and gave hints as to the head disposition (Morris et al. 1991). It was   624
mentioned earlier that modelling low-angle X-ray diffraction data from vertebrate   625
myosin filaments would be problematical if it turns out that the head organisation in   626
the C-zone is not the same as that in the P-zone and D-zone. However, it appears   627
that the IFM thick filaments are probably purely helical along most of their length.   628
In this case, application of rigorous data stripping (Rajkumar et al. 2007) and   629

Fig. 11.21 Map of a 3D reconstruction of human heart myosin filaments as in Fig. 11.20 showing a full 43 nm repeat consisting of three crowns of heads and fitted atomic structures for the myosin heads, titin (*yellow*) and C-protein (MyBP-C C8 to C10, *magenta*) (**a**). The bare zone is towards the bottom. The myosin head pair organisations in the three crowns are almost identical and the same as that in Fig. 11.18 for tarantula (Woodhead et al. 2005) and vertebrate smooth muscle heavy meromyosin (Wendt et al. 2001). The difference between crowns is that the similar head pair assemblies are rotated slightly differently as in (**b**) (Reproduced from AL-Khayat et al. 2013 with permission)

AU3
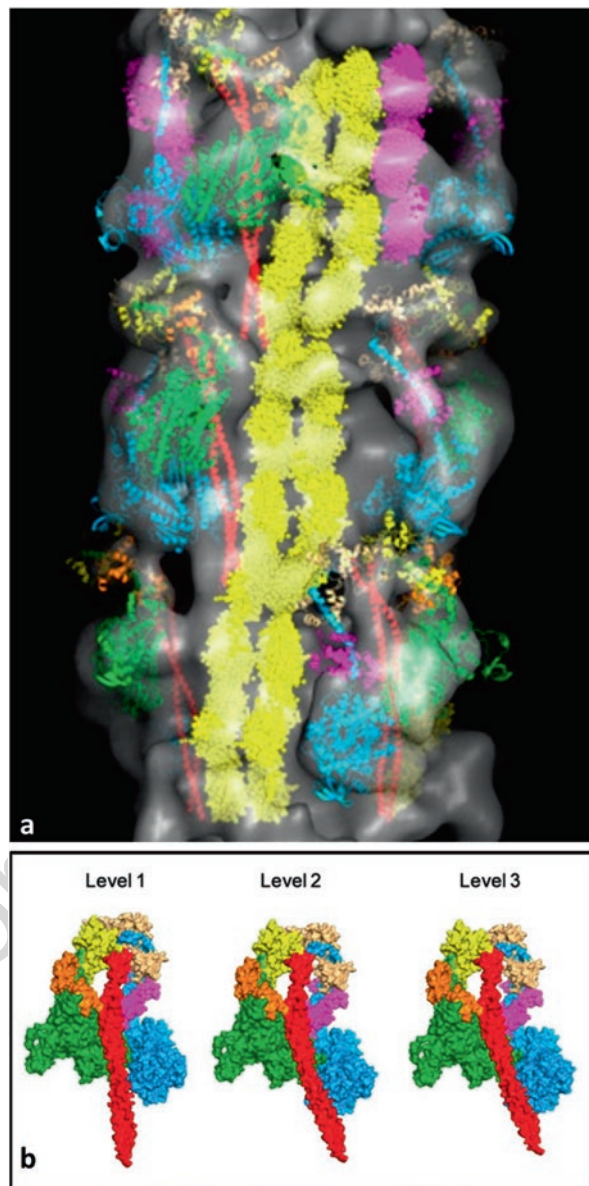
modelling methods (Hudson et al. 1997) to the beautiful IFM X-ray diffraction data
of Reedy (Figs. 11.15b and 11.22a); AL-Khayat et al. 2003), assuming perfect heli-
cal symmetry, generated a very plausible arrangement for the resting IFM myosin
heads, which is quite different from the head pairs in all the other filaments that have
been studied. The heads are apparently not in the type 1 arrangement typical of
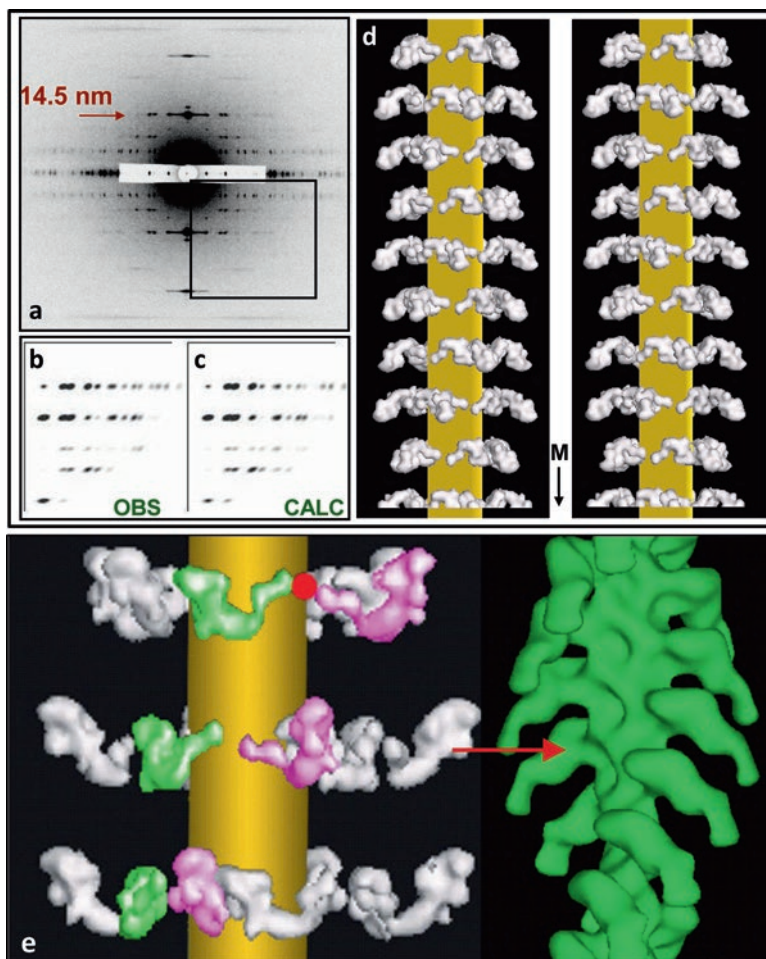
Fig. 11.22 (**a**) Low-angle X-ray diffraction pattern from insect flight muscle (*Lethocerus*) showing the lower right hand quadrant of peaks that are stripped as in (**b**) using CCP13 software ('*Fibrefix*'; Rajkumar et al. 2007) and modelled as in (**c**, **d**) by the method of Hudson et al. (1997). The calculated diffraction data (**c**) from the model in (**d**) can be compared to the original observed intensities in (**b**). (**e**) Illustration of the rather small change in motor domain orientation required for a resting head in insect flight muscle to interact with actin in rigor (*green* reconstruction to the right; Harford JJ and Squire JM unpublished data from S1-labelled fish muscle). In the insect muscle lattice the actin and myosin filaments would be much closer together, so only a small radial head movement is needed for it to attach to actin. The transition from an initial attached state to rigor would then require a large swing of the lever arm on a relatively static motor domain. Note that this figure is inverted relative to (**d**); the M-band here would be at the top (All figures reproduced from AL-Khayat et al. 2003 with permission)

635 other thick filaments, but there is a type 2 arrangement where heads from two adja-
636 cent molecules in the same crown interact with each other (Figs. 11.14f and 11.22d,
637 e). This kind of structure is supported by the fact that electron micrographs of IFM
638 thick filaments show very marked ridges or shelves of density every 14.5 nm along
639 the filaments, rather than density aligned along the long pitch helices as seen in
640 other filament types. This is also consistent with the very strong 14.5 nm meridional
641 reflection in the IFM diffraction patterns (Figs. 11.15b and 11.22a).

642   Unlike other muscles, asynchronous insect flight muscles, such as those in
643 *Lethocerus* discussed here, are designed to oscillate when activated. They display
644 the phenomenon of stretch activation, whereby the muscles pull back harder when
645 they are stretched so that together with the thorax/wing assembly to which they are
646 connected they act as a resonant mechanical system, where only the occasional
647 nervous input is needed to keep the system oscillating. As shown in AL-Khayat
648 et al. (2003), the resting myosin heads in insect flight muscle (Fig. 11.22e) appear
649 to be in a configuration whereby they could attach to actin with only a small radial
650 movement; the system appears suited to the rapid synchronous head movements
651 necessary for oscillatory contraction.

652 *11.3.6 The Myosin Filament Backbone*

653 With enormous advances in knowledge of the myosin filament symmetries in differ-
654 ent muscles and the different arrangements of the myosin heads, the remaining
655 major unknown is how the coiled-coil myosin rods are packed into the filament
656 backbone. We know from a variety of X-ray diffraction observations on the packing
657 of two-chain coiled-coils that they are about 2 nm in diameter when hydrated and
658 their centre-to-centre packing distance is about the same (e.g. Squire 1975; Elliott
659 1979). The original 'General Model of Myosin Filament Structure' by Squire (1971)
660 was based on the premise that all myosin filament surface lattices would be rather
661 similar, as they have proved to be (see Fig. 11.14), and this itself was based on the
662 idea that myosin rods would presumably pack in a certain way to give rise to the
663 related surface lattices. On this basis Squire (1973) proposed a packing scheme for
664 all types of myosin filaments based on plausible rod interactions, equivalent pack-
665 ing and able to generate the known head surface lattices. He came up with a curved
666 crystal model where the rods are fairly straight and are only slightly tilted from the
667 long axis of the myosin filaments. An example of this arrangement for 4-stranded
668 filaments is illustrated in Fig. 11.17c, where each circle represents the cross-section
669 of one myosin rod, all myosin rods are equivalent and the array produces a perfectly
670 helical surface lattice. The related structure for the 3-start filaments in vertebrate
671 striated muscle is shown in more detail in Figs. 11.23d and 11.24a taken from Chew
672 and Squire (1995).

673   This curved crystal model is not the only packing scheme that can make the
674 myosin rods equivalent. There are also a variety of myosin sub-filament models in
675 which the myosin rods first pack into sub-filaments, and then a number of similar
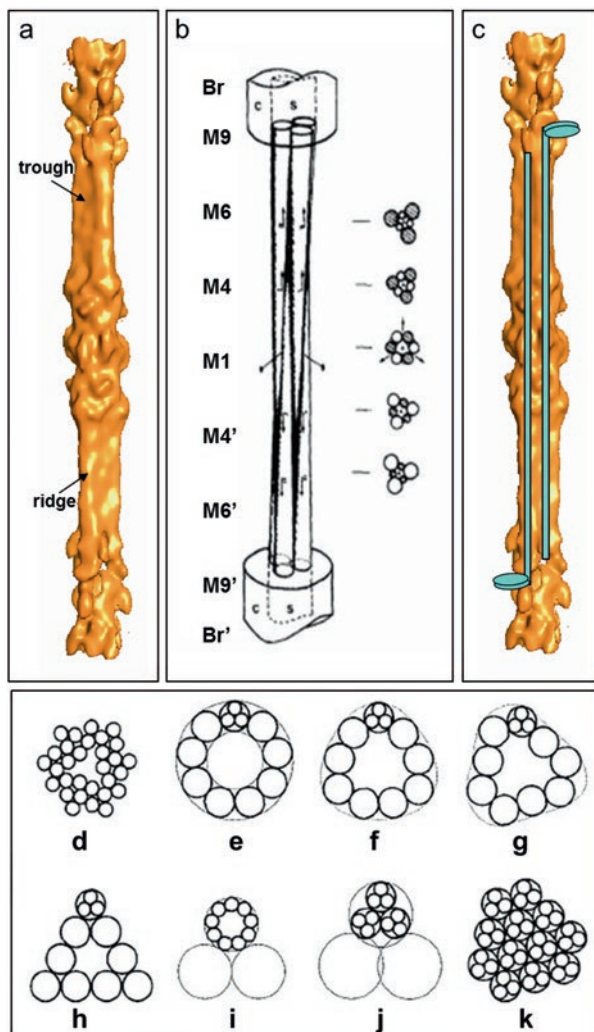
Fig. 11.23 Analysis of the bare zone of vertebrate striated muscle thick filaments. (**a**) shows a single particle reconstruction of the bare zone and start of the two bridge regions in fish skeletal muscle obtained by AL-Khayat et al. (2010). (**b**) Shows results based on an early analysis of the bare zone structure by Luther et al. (1981), suggesting that the backbone consists of three tapering densities from one end of the filament interleaved with three similar densities of opposite polarity coming from the other end of the filament. Various levels of extra M-band proteins are shown as M1 to M6, M6′ and the starts of the bridge regions are shown as Br and Br′. Results in (**a**) and (**b**) are entirely consistent. (**c**) shows how a myosin molecule (azure) might fit into the observed bare zone density. ((**a–c**) Reproduced from AL-Khayat et al. (2010) with permission). (**d–k**) Various schemes for the packing of myosin rods in the bridge regions of 3-start myosin filaments. (**d**) is a curved molecular crystal according to Squire (1973). (**e–k**) Various subfilament models for 3-start filaments. If the subfilaments have three myosin rods on average and all myosin molecules are equivalent then a large hollow ring is produced (**e**), which is not observed. The hollowness can be reduced by distorting the ring in various ways as in (**f**) to (**h**), but then the equivalence of the myosin rods is lost. The subfilaments could be larger as in (**i**), or the smaller subfilaments could be supercoiled as in (**j**) or close packed as in (**k**). Myosin rods in (**i**) and (**j**) would still be equivalent. Those in (**k**) would be far from equivalent ((**d–f**) Reproduced from Chew and Squire (1995) with permission)
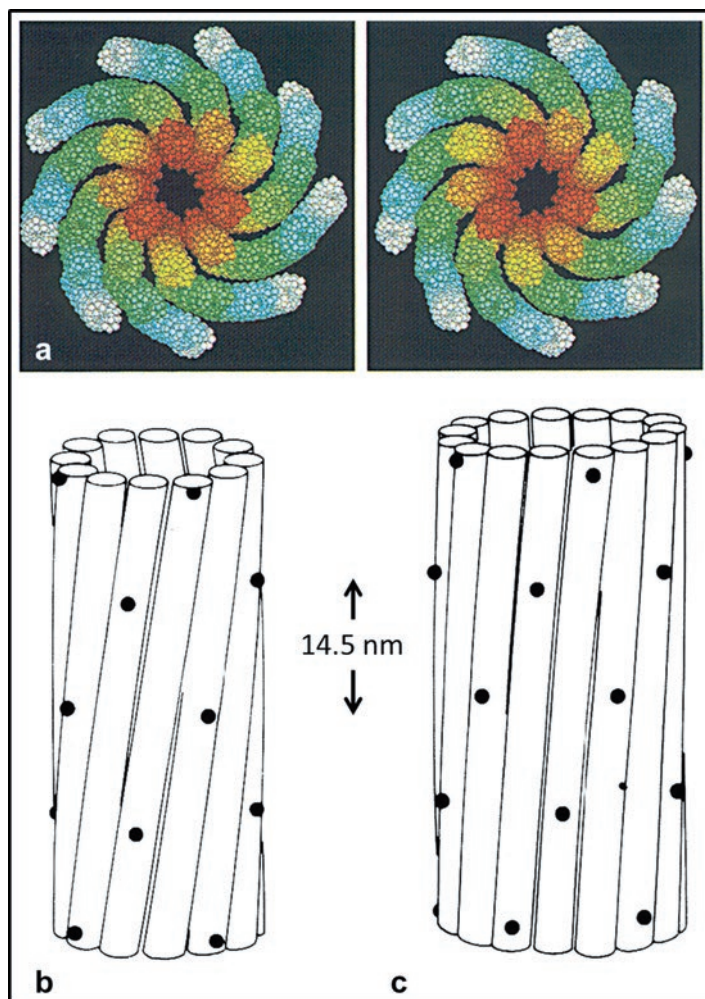
Fig. 11.24 (**a**) Stereo visualisation of the molecular crystal packing scheme proposed by Squire (1973) and shown as a simple diagram in Fig. 11.23d. Each amino acid is represented by a coloured sphere. The rods spiral down the filament at a very small angle. (**b**) and (**c**) Two possible structures for the myosin filaments in crustacean muscles (**a**) fast abdominal flexor of the lobster, (**b**) slow muscle of the lobster crusher claw. (**a**) is a 4-start filament as in other invertebrate muscles (Fig. 11.14b, c) and (**b**) a 5-start filament whose existence has not been confirmed. Sub-filament backbone structures are shown (Reproduced from Wray (1979) with permission)

676   sub-filaments pack together to form the filament backbone (Squire 1975, 1981,
677   1986; Wray 1979). Examples of this kind of structure are shown in Figs. 11.23e–k
678   and 11.24b, c. This is the structure preferred by Woodhead et al. (2005) on the basis
679   of their 3D reconstruction of Tarantula myosin filaments (Fig. 11.17d, e). A

characteristic of these sub-filament models is that they generate large empty fila- 680
ment cores (they are hollow shells) unless there is an intermediate level of coiling as 681
in Fig. 11.23j for a 3-stranded filament. 682

  The problem with these different models is that the resolution of the best myosin 683
filament reconstructions (Woodhead et al. 2005; AL-Khayat et al. 2013) is still only 684
about 2.5 nm. Since the rods pack only 2 nm apart it is very difficult to determine 685
the rod positions in the current reconstructions; real insight into myosin rod packing 686
will only come from reconstructions with significantly higher resolution. Having 687
said that, Chew and Squire (1995) suggested, after modelling high-angle (i.e. high 688
resolution) X-ray diffraction data from vertebrate muscles, the rods were very likely 689
to be almost parallel to the muscle long axis. This would be true for the curved 690
crystal model, but the rod tilt gets much bigger in some sub-filament models (Chew 691
and Squire 1995). 692

## 11.3.7   *The Vertebrate Myosin Filament Bare Zone*   693

An intriguing aspect of bipolar myosin filaments is what happens in the bare zone, 694
where the myosin rod packing is antiparallel. Squire (1973) made a suggestion 695
about how the rods might pack to give the triangular filament profile that was 696
observed in this region of the filament in cross-section. The story was then advanced 697
substantially by Luther et al. (1981) in their rigorous analysis of frog muscle cross- 698
sections, where they showed that the whole myosin filament has the symmetry of 699
the dihedral point group 32. This means that, as well as the threefold rotational sym- 700
metry intrinsic to the 3-start helical arrangement of myosin heads (Fig. 11.14a), 701
there are also three twofold rotation axes perpendicular to the long axis of the fila- 702
ment and exactly halfway along the filament in the middle of the bare zone. Rotation 703
of the whole myosin filament about one of these axes by 180° would leave the fila- 704
ment appearance unchanged. This region was then visualised in 3D by AL-Khayat 705
et al. (2010), the dihedral 32 point group symmetry was confirmed, and then this 706
symmetry was applied to the reconstruction to provide further structural averaging. 707
The final structure, Fig. 11.23a, b, was interpreted as showing three tapering densi- 708
ties more or less parallel to the filament long axis coming down from the top of the 709
Figure, interdigitating with three similar but antiparallel densities coming up from 710
the bottom end of the filament. Figure 11.23c shows how the rods might fit into 711
these densities. This scheme would explain why filament cross-sections appear 712
fairly triangular each side of the M-band (around lines M4 and M6 up to M9; 713
Fig. 11.23b), but more circular in the middle at M1, where the six tapering densities, 714
both up and down, all have the same diameter (Luther et al. 1981). Once again, more 715
resolution is needed to see how the myosin rods are actually packed, but the impli- 716
cation from this structure is that the rods are fairly parallel to the filament long axis. 717
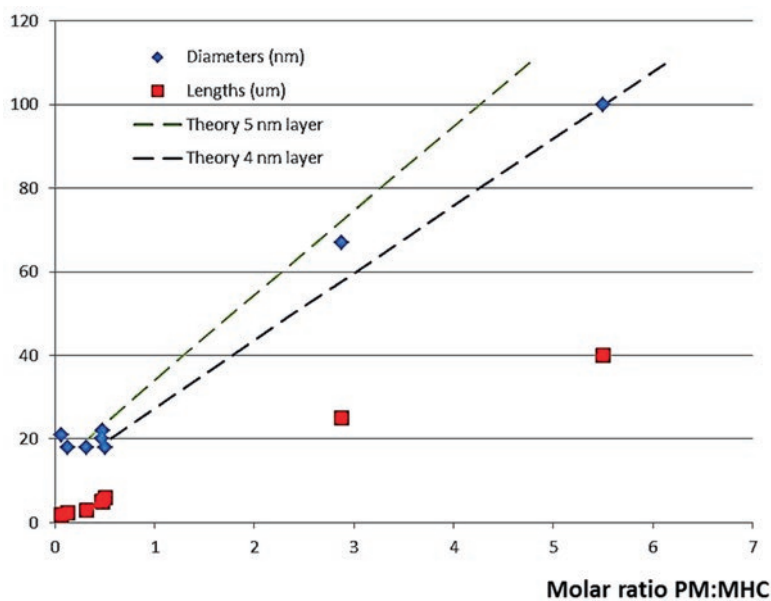
718 *11.3.8   Paramyosin Filaments*

719 The muscles of many molluscs are smooth muscles in the sense that their myosin
720 and actin filaments are not organised into regular sarcomeres. In addition, many of
721 these muscles have very large myosin-containing filaments. They are very much
722 larger in diameter than in vertebrate or insect muscles and they can be very long.
723 The bulk of these filaments is composed of the two-chain coiled-coil α–helical pro-
724 tein paramyosin, which is like the rod part of myosin, but with no myosin heads on
725 the end (Kantha et al. 1990). High-angle X-ray diffraction patterns from these fila-
726 ments have suggested that the 2 nm diameter paramyosin molecules pack into a
727 nearly tetragonal body-centred lattice about 2.7 nm on a side. There was some
728 debate about how these rods are packed on a larger scale. Elliott G.F (1964a) origi-
729 nally suggested on the basis of appearances in muscle sections that these filaments
730 might have the molecules packed into flat layers. Elliott A. and Lowy (1970) then
731 suggested that the structure night have a flat layer of molecules wrapped into a kind
732 of swiss-roll structure – giving the filaments a helicoidal arrangement of paramyo-
733 sin molecules. Further work by Elliott (A) and Bennett (1984) then confirmed that
734 Elliott G.F. had been right and that there is a flat layer structure – a structure similar
735 to synthetic aggregates studied by Cohen et al. (1971).
736 An early observation by X-ray diffraction (Bear and Selby 1956) later confirmed
737 by electron microscopy (e.g. Szent-Gyorgyi et al. 1971) was that paramyosin fila-
738 ments show a characteristic net-like surface arrangement (Fig. 11.25a, b), known as
739 the Bear-Selby net. It has the characteristic axial repeat of 14.5 nm between crowns
740 as in other myosin filaments, but here the surfaces are relatively flat and the Bear-
741 Selby net is almost a 2D lattice. The repeating units – clusters of paramyosin mol-
742 ecules – are shifted axially by 14.5 nm and laterally by differing amounts on
743 different paramyosin filaments to give a true axial repeat (the 'c' repeat; Fig. 11.24b)
744 after five of the 14.5 nm crown levels, giving a repeat of c = 72 nm. The variable
745 lateral spacing in the Bear-Selby net is usually termed the 'a' spacing (Fig. 11.25b).
746 The results of Elliott (1979) and Elliott and Bennett (1984) clearly showed that if
747 paramyosin filaments showing the Bear-Selby net pattern are rotated around their
748 long axes then the net pattern tends to disappear and a simple 14.5 nm axial banding
749 is obtained. Their preferred structure is as in Fig. 11.25c–e. Figure 11.25d shows
750 how stain might accumulate between the molecular ends to give the stain patches
751 which show up the Bear-Selby net (Fig. 11.25a).
752 Squire (1971) discussed what a layer of myosin molecules might be like on the
753 surface of a roughly cylindrical backbone of paramyosin (Fig. 11.25e). Figure 11.26
754 shows the correlation between the lengths and diameters of paramyosin filaments
755 and the molar ratio of paramyosin to myosin heavy chain as determined by Levine
756 et al. (1976). The measurements appear to fit with a myosin layer of between 4 and
757 5 nm thickness as expected. The odd thing is that if the net is like one of the arrange-
758 ments in Fig. 11.14a–d, but with a 72 nm axial repeat, the interaction which such a
759 layer would make with the underlying paramyosin molecules would sometimes be
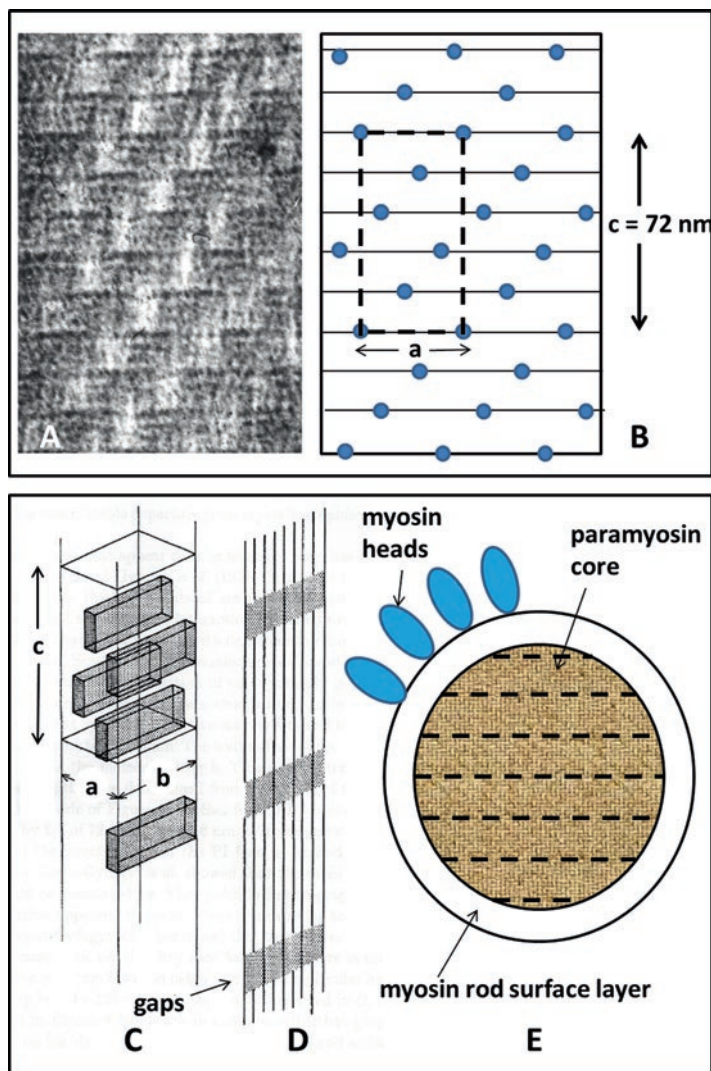
Fig. 11.25 (a) The surface lattice of paramyosin filaments as visualised in negative stain showing the Bear-Selby net pattern (Bear and Selby 1956). Features of the pattern are summarised in (**b**). (**c, d**) Three-dimensional perspective drawing of the paramyosin packing model of Elliott (1979) showing regions of stain extending through a filament. The 'b' direction is normal to the plane through 'a' and 'c'. (**b**) Diagrammatic perspective representation showing a single layer of para-myosin molecules from (**c**) each (l = ????) 129.1 nm long with an axial displacement of c = 72 nm between neighbours (as in Cohen et al. (1971)). Stain can lodge in gaps 72 nm apart between the ends of the molecules [(**c, d**) Reproduced from Elliott (1979) with permission]. (**e**) Illustration of a paramyosin filament cross-section with a central layered paramyosin structure and a surface layer of myosin rods from which myosin heads (*blue*) project

Fig. 11.26 Plots of the measured diameters and lengths of paramyosin filaments from a variety of sources plotted against the molar paramyosin to myosin heavy chain ratio as determined by Levine et al. (1976). The observed diameters (*blue diamonds*) are consistent with a myosin layer of thickness about 4–5 nm – *dashed lines*

760 with a Bear-Selby net structure and sometimes with a structure which has simple
761 14.5 nm axial banding. Is that plausible, or is it, for example, only the Bear-Selby
762 net face that carries myosin?

763 ### 11.3.9 Myosin Filaments in Vertebrate Smooth Muscles

764 The last two sections here are about myosin filaments that do not fit to the standard
765 patterns found in other muscles as discussed so far. The first are the myosin fila-
766 ments in vertebrate smooth muscles. In the 1950s and 1960s, when the first electron
767 micrographs of striated muscles were obtained, vertebrate intestinal and other vis-
768 ceral muscles were also studied. It was confirmed that, unlike striated muscles, there
769 were no sarcomeres present, but the surprising result was also found that there were
770 no myosin filaments apparent in these muscles (e.g. Shoenberg 1969). Eventually it
771 was assumed that vertebrate smooth muscle myosin filaments must be present when
772 the muscles are active, but that they may assemble as needed from a pool of myosin
773 molecules in inactive muscles. Attempts were then made to find conditions under
774 which smooth muscles myosin molecules would assemble into filaments that could
775 be visualised. The breakthrough came with the study of guinea pig *Taenia coli* mus-
776 cles (from along the large intestine) when treated with hypertonic Ringer solution
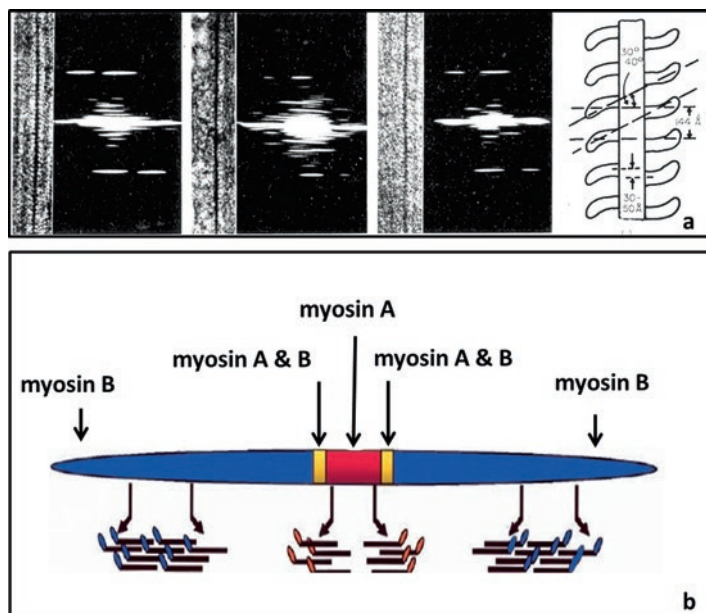
Fig. 11.27 (**a**) Myosin filaments (*left images* in each pair) in vertebrate smooth muscle seen in edge view and the corresponding asymmetrical optical diffraction pattern. This shows the presence of face polar (side polar) arrangements of projecting myosin heads in which heads on opposite faces point towards opposite ends of the filaments, as summarised in the *right hand figure* (Figure Reproduced from Small and Squire (1972) with permission). (**b**) The distribution of myosins A and B in the bipolar thick filaments of C. elegans body wall muscle (Modified from Landsverk and Epstein 2005)

(Lowy et al. 1970; Vibert et al. 1971). Under these conditions (slightly stronger than normal Ringer solution) a very clear 14.4 nm meridional X-reflection characteristic of the presence of myosin filaments was observed (Vibert et al. 1971). A meridional reflection at 0.51 nm, characteristic of oriented α–helical rods (presumably mainly myosin rods) was also seen. Then, in a major electron microscopy study of thin sections of *Taenia coli* (Small and Squire 1972), the myosin filaments themselves were observed and analysed. However, they were definitely not bipolar filaments as found in striated muscles. The myosin aggregates that were observed were ribbon-shaped and very long. They were called myosin ribbons. Image analysis of edge views of the sectioned filaments clearly showed that the projecting myosin heads on the 14.4 nm repeat were not pointing in the same direction on each side of the filament as would occur in a bipolar filament (Fig. 11.27a), but heads on one side of the filament pointed towards the opposite end of the ribbon to the heads on the other side (Fig 11.27a right hand image). This was termed face polarity and, as detailed in Small and Squire (1972), this structure enabled smooth muscles to operate over a very large range of muscle lengths, since the interacting actin filaments, which were very long, would move in opposite directions on opposite faces of the myosin ribbons. The face polarity was confirmed by image analysis of the edge view ribbon

795 projections where a characteristic optical diffraction pattern was obtained. Instead
796 of showing peaks on each side of the meridional reflection at 14.4 nm, as might be
797 expected for a bipolar filament, the ribbons gave a pattern where the 14.4 nm peak
798 had an additional reflection on the same layer line but on one side of the meridian
799 only. Looking at the top part of the pattern, if the extra peak on the 14.4 nm layer
800 line was on the left, then on the bottom it was on the right (Fig. 11.27a).

801 Since that time it has been found that the filaments in this muscle are normally
802 not as wide as the ribbons seen by Small and Squire (e.g. Somlyo et al. 1973), but
803 the same kind of opposite polarity on opposite faces of smaller filaments was seen
804 in aggregates of pure smooth muscle myosin (Craig and Megerman 1977; Xu et al.
805 1996). These smaller filaments with a roughly square backbone profile were termed
806 side-polar, but this was an unnecessary and misleading name. A square prism has
807 faces, so face-polarity would remain the correct term irrespective of the filament
808 width. The physiological advantages of this kind of polarity, even if the filaments
809 are termed side-polar, are identical to those detailed by Small and Squire (1972).
810 The smaller filaments may just aggregate under some conditions to produce the
811 wider ribbons (e.g. Somlyo et al. 1973).

812 Small and Squire (1972) originally thought it possible that the ribbons might
813 have a backbone core consisting of the 10 nm (intermediate) filaments that were
814 seen in abundance in the *Taenia coli* sections. However, this is not the case since
815 filaments with side- or face- polarity can be generated from a pure preparation of
816 smooth muscle myosin (Craig and Megerman 1977). The presence of face-polarity
817 rather than bipolarity can also be explained in terms of the different amino acid
818 sequences in myosins from striated and smooth muscles (Straussman et al. 2005).
819 The intermediate filaments form a separate cytoskeletal network in smooth muscle
820 cells (Small and Sobieszek 1977).

821 A recent survey of face-polar or side-polar filaments in vertebrate smooth mus-
822 cles has shown considerable variability in length between muscles and muscle
823 states, and the suggestion was made that filaments are in equilibrium with myosin
824 dimers and that they assemble or disassemble as required (Liu et al. 2013).

11.3.10   *Nematode and* Limulus *Muscles*

826 The nematode *Caenorhabditis elegans* (C. elegans) has great advantages in carrying
827 out genetic studies and has been widely used for a variety of purposes (Brenner
828 1974). Along with *Drosophila* and Zebra fish, it provides a method of genetic dis-
829 section and in vivo development in the study of muscle structure and behaviour (e.g.
830 Barral and Epstein 1999; Landsverk and Epstein 2005). The thick filaments in the
831 body wall muscle have two types of myosin with heavy chains A and B, together
832 with paramyosin. The two myosins are distributed in a particular way in the bipolar
833 thick filament (Fig. 11.27b). The central region is entirely myosin A, there are then

small transition regions with both myosins A and B, and then the peripheral parts of the filament are entirely composed of myosin B. The structure of the filament backbone and the head organisation are not really known, although some suggestions have been made (e.g. Müller et al. 2001). Further work is needed to position this filament into the family of other thick filaments.

The story of *Limulus* telson muscle thick filaments is rather different. The thick filaments appear relatively normal compared to those in other muscles in that they are bipolar and their heads lie on 4-start helices (Figs. 11.14b and 11.16b; Wray et al. 1974; Stewart et al. 1981; Zhao et al. 2009). What is different about these filaments is how they behave as the sarcomere length in the muscles changes. An advantage for some muscles is that they operate over a wide range of sarcomere lengths. With the normal ideas about the muscle sarcomere and the sliding filament mechanism (Fig. 11.1a), only a limited range of filament sliding can occur. This is especially true on shortening of the muscle when first the actin filaments penetrate the M-band and then, on further shortening, the myosin filaments collide with the Z-band. However, there is evidence that the myosin filaments in *Limulus* are designed in such a way that the myosin filament tips collapse by losing molecules when they approach the Z-band, thus allowing the *Limulus* muscles to shorten more than usual and therefore to operate over a wider sarcomere length range than normal (Dewey et al. 1977). No doubt further anomalous behaviours will become apparent when other myosin filaments are studied.

11.4   Future Prospects

Enormous progress has been made since Huxley first isolated myosin filaments from muscle. We now know the lattice symmetries and head arrangements in a number of muscles in some detail, but we still do not know how the myosin rods pack. In the case of the thin filament, results are starting to emerge on the arrangement of troponin and the individual tropomyosin repeats within a regulatory unit. But, as in many such studies, the big thing is to improve the resolution of the reconstructions that are produced. Only then will we know how these filaments are made and how they work.

Recent developments in detector technology already allow for the determination of the structure of protein complexes by cryo-electron microscopy at a resolution as high as 2.2 Å (Bartesaghi et al. 2015), and it is likely that even higher resolution structures of appropriate complexes will be obtained in the near future. It seems probable, therefore, that cryo-electron microscopy and single particle analysis could be used to obtain much higher resolution structures than are currently available for both thick and thin muscle filaments, although this will also require substantial improvements in sample preparation.

11.5   Late Breaking Results

After the bulk of this chapter was written, the authors heard of the ground-breaking work of Hu et al. (2016) who have used electron microscopy and single particle analysis to define the structure of the thick filaments from insect flight muscle (*Lethocerus*). They found that the myosin head arrangement at about 2 nm resolution was exactly the same as in other muscles in being of the type shown in Figs. 11.18 and 11.21b. But as in Fig. 11.22, the head pairs were not close to the filament surface, but were angled so that the plane of the head density was fairly flat on each 14.5 nm spaced crown to give the shelves of density characteristic of insect flight muscle thick filaments. Even more remarkable in this work is that the backbone structure is revealed at about 0.6 nm resolution. This is sufficient to see the individual myosin rods. They found that at intermediate resolution there appeared to be sub-filaments, as has been suggested before, However, at the full 0.6 nm resolution, there were no sub-filaments and the rod packing was exactly as in Fig. 11.17c for a 4-stranded filament (Squire 1973). It is likely that other kinds of myosin filament also have this kind of molecular crystal packing.

References

Ababou A, Rostkova E, Mistry S, Le Masurier C, Gautel M, Pfuhl M (2008) Myosin binding protein C positioned to play a key role in regulation of muscle contraction: structure and interactions of domain C1. J Mol Biol 384:615–630

Agarkova I, Perriard JC (2005) The M-band: an elastic web that crosslinks thick filaments in the center of the sarcomere. Trends Cell Biol 15:477–485

Alamo L, Wriggers W, Pinto A, Bartoli F, Salazar L, Zhao FQ, Craig R, Padron R (2008) Three-dimensional reconstruction of tarantula myosin filaments suggests how phosphorylation may regulate myosin activity. J Mol Biol 384:780–797

AL-Khayat HA, Squire JM (2006) Refined structure of bony fish muscle myosin filaments from low-angle X-ray diffraction data. J Struct Biol 155:218–229

AL-Khayat HA, Yagi N, Squire JM (1995) Structural changes in actin-tropomyosin during muscle regulation: computer modelling of low-angle X-ray diffraction data. J Mol Biol 252:611–632

AL-Khayat HA, Hudson L, Reedy MK, Irving TC, Squire JM (2003) Myosin head configuration in relaxed insect flight muscle: X-ray modelled resting cross-bridges in a pre-powerstroke state are poised for actin binding. Biophys J 85:1063–1079

AL-Khayat HA, Morris EP, Squire JM (2004) Single particle analysis: a new approach to solving the 3D structure of myosin filaments. J Mus Res Cell Motil 25:635–644

AL-Khayat HA, Morris EP, Powell AS, Kensler RW, Squire JM (2006) 3D structure of vertebrate (fish) muscle myosin filaments by single particle analysis. J Struct Biol **155**:202–217

AL-Khayat HA, Morris EP, Kensler RW, Squire JM (2008) 3D structure of relaxed mammalian (rabbit) cardiac muscle myosin filaments by electron microscopy and single particle analysis. J Struct Biol 163:117–126

AL-Khayat HA, Morris EP, Squire JM (2009a) The 7-stranded structure of relaxed scallop muscle myosin filaments: support for a common head configuration in myosin-regulated muscles. J Struct Biol **166**:183–194

AL-Khayat HA, Morris EP, Squire JM (2009b) 3D structure of relaxed scallop striated muscle myosin filaments by electron microscopy and single particle analysis. J Struct Biol 166:183–194

AL-Khayat HA, Kensler RW, Morris EP, Squire JM (2010) Three-dimensional structure of the M-region (bare zone) of vertebrate striated muscle myosin filaments by single-particle analysis. J Mol Biol 403:763–776

AL-Khayat HA, Kensler RW, Squire JM, Marston SB, Morris EP (2013) Atomic model of the human cardiac muscle myosin filament. Proc Natl Acad Sci U S A 110:318–323

Barral JM, Epstein HF (1999) Protein machines and self-assembly in muscle organization. BioEssays 21:813–823

Bartesaghi A, Merk A, Banerjee S, Matthies D, Wu X, Milne JL, Subramaniam S (2015) 2.2 Å resolution cryo-EM structure of β-galactosidase in complex with a cell-permeant inhibitor. Science 348:1147–1151

Bear RS, Selby CC (1956) The structure of paramyosin fibrils according to X-ray diffraction. J Biophys Biochem Cytol 2:55–69

Behrmann E, Muller M, Penczek PA, Mennherz HG, Manstein DJ, Raunser S (2012) Structure of the rigor actin-tropomyosin-myosin complex. Cell 150:327–338

Bennett P, Craig R, Starr R, Offer G (1986) The ultrastructural location of C-protein, X-protein and H-protein in rabbit muscle. J Muscle Res Cell Motil 7:550–567

Bremel RD, Weber A (1972) Cooperation within actin filament in vertebrate skeletal muscle. Nat New Biol 238:97–101

Brenner S (1974) The genetics of *Caenorhabditis elegans*. Genetics 77:71–94

Brown JH, Cohen C (2005) Regulation of muscle contraction by tropomyosin and troponin: how structure illuminates function. 'Muscle & molecular motors' (Ed Squire JM, Parry DAD). Adv Protein Chem 71:121–159.

Caspar DL, Cohen C, Longley W (1969) Tropomyosin: crystal structure, polymorphism and molecular interactions. J Mol Biol 41:87–107

Chew MW, Squire JM (1995) Packing of alpha-helical coiled-coil myosin rods in vertebrate muscle thick filaments. J Struct Biol 115:233–249

Clarke M, Hoffman W, Wray JS (1986) ATP binding and crossbridge structure in muscle. J Mol Biol 191:581–585

Cohen C, Szent-Györgyi AG, Kendrick-Jones J (1971) Paramyosin and the filaments of molluscan "catch" muscles. I. Paramyosin: structure and assembly. J Mol Biol 56:223–227

Craig R, Megerman J (1977) Assembly of smooth muscle myosin into side polar filaments. J Cell Biol 75:990–996

Craig R, Woodhead J (2006) Structure and function of myosin filaments. Curr Opin Struct Biol 16:204–212

Craig R, Lee KH, Mun JY, Torre I, Luther PK (2014) Structure, sarcomeric organization, and thin filament binding of cardiac myosin-binding protein-C. Pflugers Arch 466:425–431

Craig R, Padron R, Alamo L (1991) Direct determination of myosin filament symmetry in scallop striated adductor muscle by rapid freezing and freeze substitution. J Mol Biol 220:125–132

Crowther RA, Padron R, Craig R (1985) Arrangement of the heads of myosin in relaxed thick filaments from tarantula muscle. J Mol Biol 182:429–439

DeRosier DJ, Klug A (1968) Reconstruction of three-dimensional structures from electron micrographs. Nature 217:130–134

DeRosier DJ, Moore P (1971) Reconstruction of three-dimensional images from electron micrographs of structures with helical symmetry. J Mol Biol 52:355–369

913
914
915
916
917
918
919
920
921
922
923
924
925
926
927
928
929
930
931
932
933
934
935
936
937
938
939
940
941
942
943
944
945
946
947
948
949
950
951
952
953
954
955
956
957
958
959
960
961
962
963
964
965

966 Dewey MM, Walcott B, Colflesh DE, Terry H, Levine RJC (1977) Changes in thick filament length
967   in Limulus striated muscle. J Cell Biol 75:366–380
968 Dominguez R, Freyzon Y, Trybus KM, Cohen C (1998) Crystal structure of a vertebrate smooth
969   muscle myosin motor domain and its complex with the essential light chain: visualization of
970   the pre-powerstroke state. Cell 94:559–571
971 Ebashi S, Endo M (1968) Calcium ion and muscle contraction. Prog Biophys Mol Biol
972   18:123–183
973 Egelman EH (2000) A robust algorithm for the reconstruction of helical filaments using single-
974   particle methods. Ultramicroscopy 85:225–234
975 Elliott GF (1964a) Electron microscope studies of the structure of the filaments in the opaque
976   adductor muscle of the oyster *Crassostrea Angulata*. J Mol Biol 10:89–104
977 Elliott GF (1964b) X-ray diffraction studies on striated and smooth muscles. Proc R Soc Lond B
978   Biol Sci 160:467–472
979 Elliott GF (1967) Variations of the contractile apparatus in smooth and striated muscles: X-ray
980   diffraction studies at rest and in contraction. J Gen Physiol 50(Suppl):171–184
981 Elliott A (1979) Structure of molluscan thick filaments: a common origin for diverse appearances.
982   J Mol Biol 132:323–340
983 Elliott A, Bennett P (1984) Molecular organization of paramyosin in the core of molluscan thick
984   filaments. J Mol Biol 176:477–493
985 Elliott A, Lowy J (1970) A model for the coarse structure of paramyosin filaments. J Mol Biol
986   53:181–203
987 Frank J, Radermacher M, Penczek P, Zhu J, Li Y, Ladjadj M, Leith A (1996) SPIDER and WEB:
988   processing and visualization of images in 3D electron microscopy and related fields. J Struct
989   Biol 116:190–199
990 Fujii T, Iwane AH, Yanagida T, Namba K (2010) Direct visualization of secondary structures of
991   F-actin by electron cryomicroscopy. Nature 467:724–728
992 Fusi L, Huang Z, Irving M (2015) The conformation of myosin heads in relaxed skeletal muscle:
993   implications for myosin-based regulation. Biophys J 109:783–792
994 Govada L, Carpenter L, da Fonseca PCA, Helliwell JR, Rizkallah P, Flashman E, Chayen NE,
995   Redwood C, Squire JM (2008) Crystal structure of the C1 domain of cardiac myosin binding
996   protein-C: implications for hypertrophic cardiomyopathy. J Mol Biol 378:387–397
997 Granzier HL, Labeit S (2005) Titin and its associated proteins. In 'Muscle & molecular motors'.
998   (Ed Squire JM, Parry DAD). Adv Protein Chem 71: 89–119.
999 Granzier HL, Labeit S (2007) Structure-function relations of the giant elastic protein titin in stri-
1000   ated and smooth muscle cells. Muscle Nerve 36:740–755
1001 Hanson J, Lowy J (1963) The structure of F-actin and of actin filaments isolated from muscle.
1002   J Mol Biol 6:46–60
1003 Hardwicke PM, Hanson J (1971) Separation of thick and thin myofilaments. J Mol Biol
1004   59:509–516
1005 Harford J, Squire JM (1986) "Crystalline" myosin cross-bridge array in relaxed bony fish muscle.
1006   Low-angle X-ray diffraction from plaice fin muscle and its interpretation. Biophys
1007   J 50:145–155
1008 Haselgrove JC (1972) X-ray evidence for a conformational change in actin-containing filaments of
1009   vertebrate striated muscle. Cold Spring Harb Symp Quant Biol 37:341–352
1010 Houdusse A, Szent-Gyorgyi AG, Cohen C (2000) Three conformational states of scallop myosin
1011   S1. Proc Natl Acad Sci 97:11238–11243
1012 Holmes KC, Lehman W (2008) Gestalt-binding of tropomyosin to actin filaments. J Muscle Res
1013   Cell Motil 29:213–219
1014 Holmes KC, Popp D, Gebhard W, Kabsch W (1990) Atomic model of the actin filament. Nature
1015   347:44–49
1016 Holmes KC, Schröder RR, Sweeney HL, Houdusse A (2004) The structure of the rigor complex
1017   and its implications for the power stroke. Philos Trans R Soc Lond Ser B Biol Sci
1018   359:1819–1828

Hu Z, Taylor DW, Reedy MK, Edwards RJ, Taylor KA (2016) Structure of myosin filaments from relaxed Lethocerus flight muscle by cryo-em at 6 Å resolution. Sci Adv 2(9):e1600058

Hudson L, Harford JJ, Denny RC, Squire JM (1997) Myosin head configuration in relaxed fish muscle: resting state myosin heads must swing axially by up to 150 Å or turn upside down to reach rigor. J Mol Biol 273:440–455

Huxley AF, Niedergerke R (1953) Structural changes in muscle during contraction: interference microscopy of living muscle fibres. Nature 173:971–973

Huxley HE (1963) Electron microscope studies on the structure of natural and synthetic protein filaments from striated muscle. J Mol Biol 7:281–308

Huxley HE (1969) The mechanism of muscular contraction. Science 164:1356–1365

Huxley HE (1972) Structural changes in actin- and myosin-containing filaments during contraction. Cold Spring Harb Symp Quant Biol 37:361–376

Huxley HE, Hanson EJ (1953) Structural basis of the cross-striations in muscle. Nature 172:530–532

Huxley HE, Brown W (1967) The low-angle X-ray diagram of vertebrate striated muscle and its behaviour during contraction and rigor. J Mol Biol 30:383–434

Jung SK, Komatsu S, Ikebe M, Craig R (2008b) Head-head and head-tail interaction: a general mechanism for switching off myosin II activity in cells. Mol Biol Cell 19:3234–3242

Jung SK, Burgess SA, Billington N, Colegrave M, Patel H, Chalovich JM, Chantler PD, Knight PJ (2008a) Conservation of the regulated structure of folded myosin 2 in species separated by at least 600 million years of independent evolution. PNAS 105:6022–6026

Kabsch W, Mannherz HG, Suck D, Pai EF, Holmes KC (1990) Atomic structure of the actin: DNase I complex. Nature 347:37–44

Kampourakis T, Yan Z, Gautel M, Sun YB, Irving M (2015) Myosin binding protein-C activates thin filaments and inhibits thick filaments in heart muscle cells. Proc Natl Acad Sci U S A 111:18763–18768

Kantha SS, Watabe S, Hashimoto K (1990) Comparative biochemistry of paramyosin – a review. J Food Biochem 14:61–88

Kensler RW, Harris SP (2008) The structure of isolated cardiac myosin thick filaments from cardiac myosin binding protein C knockout mice. Biophys J 94:1707–1718

Kensler RW, Stewart M (1983) Frog skeletal muscle thick filaments are three-stranded. J Cell Biol 96:1797–1802

Knupp C, Luther PK, Squire JM (2002) Titin organisation and the 3D architecture of the vertebrate-striated muscle I-band. J Mol Biol 322:731–739

Kuhlbrandt W (2014) The resolution revolution. Science 343:1443–1444

Kulikovskaya I, McClellan G, Flavigny J, Carrier L, Winegrad S (2003) Effect of MyBP-C binding to actin on contractility in heart muscle. J Gen Physiol 122:761–774

Kunst G, Kress KR, Gruen M, Uttenweiler D, Gautel M, Fink RH (2000) Myosin binding protein C, a phosphorylation-dependent force regulator in muscle that controls the attachment of myosin heads by its interaction with myosin S2. Circ Res 86:51–58

Landsverk ML, Epstein HF (2005) Genetic analysis of myosin II assembly and organization in model organisms. Cell Motil Life Sci 62:2270–2282

Lehman W, Craig R, Vibert P (1994) Ca(2+)-induced tropomyosin movement in Limulus thin filaments revealed by three-dimensional reconstruction. Nature 368:65–67

Lehman W, Vibert P, Uman P, Craig R (1995) Steric-blocking by tropomyosin visualized in relaxed vertebrate muscle thin filaments. J Mol Biol 251:191–196

Lehrer SS, Morris EP (1982) Dual effects of tropomyosin and troponin-tropomyosin on actomyosin subfragment 1 ATPase. J Biol Chem 257:8073–8080

Lehrer SS, Geeves MA (1998) The muscle thin filament as a classical cooperative/allosteric regulatory system. J Mol Biol 277:1081–1089

Levine RJC, Elfvin M, Dewey MM, Walcott B (1976) Paramyosin in invertebrate muscles II Content in relation to structure and function. J Cell Biol 71:273–279

1071 Li XE, Tobacman LS, Mun JY, Craig R, Fischer S, Lehman W (2011) Tropomyosin position on
1072   F-actin revealed by EM reconstruction and computational chemistry. Biophys
1073   J 100:1005–1013
1074 Liu JCY, Rottler J, Wang L, Zhang J, Pascoe CD, Lan B, Norris BA, Herrera AM, Paré PD, Seow
1075   CY (2013) Myosin filaments in smooth muscle cells do not have a constant length. J Physiol
1076   591:5867–5878
1077 Liversage AD, Holmes D, Knight PJ, Tskhovrebova L, Trinick J (2001) Titin and the sarcomere
1078   symmetry paradox. J Mol Biol 305:401–409
1079 Lowy J, Hanson J (1962) Ultrastructure of invertebrate smooth muscles. Physiol Rev Suppl
1080   5:34–47
1081 Lowey S, Slayter HS, Weeds AG, Baker H (1969) Substructure of the myosin molecule.
1082   I. Subfragments of myosin by enzymic degradation. J Mol Biol 42:1–29
1083 Lowy J, Poulsen FR, Vibert J (1970) Myosin filaments in vertebrate smooth muscle. Nature
1084   225:1053–1054
1085 Ludtke SJ, Baldwin PR, Chiu W (1999) EMAN: semi-automated software for high-resolution
1086   single-particle reconstructions. J Struct Biol 128:82–97
1087 Luther PK, Craig R (2011) Modulation of striated muscle contraction by binding of myosin bind-
1088   ing protein C to actin. BioArchitecture 1:277–283
1089 Luther PK, Munro PMG, Squire JM (1981) Three-dimensional structure of the vertebrate muscle
1090   A-band III: M-region structure and myosin filament symmetry. J Mol Biol 151:703–730
1091 Luther PK, Bennett PM, Knupp C, Craig R, Padrón R, Harris SP, Patel J, Moss RL (2008)
1092   Understanding the organisation and role of myosin binding protein C in normal striated muscle
1093   by comparison with MyBP-C knockout cardiac muscle. J Mol Biol 384:60–72
1094 Luther PK, Winkler H, Taylor K, Zoghbi ME, Craig R, Padrón R, Squire JM, Liu J (2011) Direct
1095   visualization of myosin-binding protein C bridging myosin and actin filaments in intact mus-
1096   cle. Proc Natl Acad Sci U S A 108:11423–11428
1097 Lymn RW, Taylor EW (1971) Mechanism of adenosine triphosphate hydrolysis by actomyosin.
1098   Biochemistry 10:4617–4624
1099 Manning EP, Tardiff JC, Schwartz SD (2011) A model of calcium activation of the cardiac thin fila-
1100   ment. Biochemistry 50:7405–7413
1101 Maw MC, Rowe AJ (1980) Fraying of A-filaments into three subfilaments. Nature 286:412–414
1102 McLachlan and Stewart, 1976
1103 Menetret JF, Schroder RR, Hofmann W (1990) Cryo-electron microscopic studies of relaxed stri-
1104   ated muscle thick filaments. J Mus Res Cell Motil 11:1–11
1105 McElhinny AS, Kolmerer B, Fowler VM, Labeit S, Gregorio CC (2001) The N-terminal end of
1106   nebulin interacts with tropomodulin at the pointed ends of the thin filaments. J Biol Chem
1107   276:583–592
1108 McKillop DF, Geeves MA (1993) Regulation of the interaction between actin and myosin subfrag-
1109   ment 1: evidence for three states of the thin filament. Biophys J 65:693–701
1110 Millman BM, Bennett PM (1976) Structure of the cross-striated adductor muscle of the scallop.
1111   J Mol Biol 103:439–467
1112 Mok, NS. (2005) X-ray diffraction studies of defined states in fish muscle. PhD Thesis, Imperial
1113   College London.
1114 Moore PB, Huxley HE, DeRosier DJ (1970) Three-dimensional reconstruction of F-actin, thin fila-
1115   ments and decorated thin filaments. J Mol Biol 50:279–295
1116 Morris EP, Squire JM, Fuller GW (1991) The 4-stranded helical arrangement of myosin heads on
1117   insect (*Lethocerus*) flight muscle thick filaments. J Struct Biol 107:237–249
1118 Moss RL, Fitzsimons DP, Ralphe JC (2015) Cardiac MyBP-C regulates the rate and force of con-
1119   traction in mammalian myocardium. Circ Res 116:183–192
1120 Müller SA, Häner M, Ortiz I, Aebi U, Epstein HF (2001) STEM analysis of Caenorhabditis ele-
1121   gans muscle thick filaments: evidence for microdifferentiated substructures. J Mol Biol
1122   305:1035–1044

Offer G, Moos C, Starr R (1973) A new protein of the thick filaments of vertebrate skeletal myofibrils. Extractions, purification and characterization. J Mol Biol 74:653–676

Offer G, Knight PJ, Burgess S, Alamo L, Padron R (2000) A new model for the surface arrangement of myosin molecules in tarantula thick filaments. J Mol Biol 298:239–260

Ohtsuki I (1979) Molecular arrangement of troponin-T in the thin filament. J Biochem 86:491–497

Ottenheijm CA, Buck D, de Winter JM, Ferrara C, Piroddi N, Tesi C, Jasper JR, Malik FI, Meng H, Stienen GJ, Beggs AH, Labeit S, Poggesi C, Lawlor MW, Granzier H (2013) Deleting exon 55 from the nebulin gene induces severe muscle weakness in a mouse model for nemaline myopathy. Brain 136:1718–1731

Otterbein LR, Graceffa P, Dominguez R (2001) The crystal structure of uncomplexed actin in the ADP state. Science 293:708–711

Parry, 1975

Parry DAD, Squire JM (1973) Structural role of tropomyosin in muscle regulation: analysis of the X-ray diffraction patterns from relaxed and contracting muscles. J Mol Biol 75:33–55

Patwardhan A, Paul D, HA AL-K, EP M (2004) A measure for the angle between projections based on the extent of correlation between corresponding central sections. J Mol Biol 344:707–724

Paul DM, Patwardhan A, Squire JM, Morris EP (2004) Single particle analysis of filamentous and highly elongated macromolecular assemblies. J Struct Biol 148:236–250

Paul DM, Squire JM, Morris EP (2016) Relaxed and active thin filament structures reveal a new regulatory mechanism: varying tropomyosin shifts within a regulatory unit

Phillips GN Jr, Fillers JP, Cohen C (1986) Tropomyosin crystal structure and muscle regulation. J Mol Biol 192:111–131

Pirani A, Xu C, Hatch V, Craig R, Tobacman LS, Lehman W (2005) Single particle analysis of relaxed and activated muscle thin filaments. J Mol Biol 346:761–772

Poole KJ, Lorenz M, Evans G, Rosenbaum G, Pirani A, Craig R, Tobacman LS, Lehman W, Holmes KC (2006) A comparison of muscle thin filament models obtained from electron microscopy reconstructions and low-angle X-ray fibre diagrams from non-overlap muscle. J Struct Biol 155:273–284

Previs MJ, Prosser BL, Mun JY, Previs SB, Gulick J, Lee K, Robbins J, Craig R, Lederer WJ, Warshaw DM (2015) Myosin-binding protein C corrects an intrinsic inhomogeneity in cardiac excitation-contraction coupling. Sci Adv 1:e1400205

Rajkumar G, HA AL-K, Eakins F, Knupp C, JM S (2007) The CCP13 Fibrefix program suite: semi-automated analysis of diffraction patterns from non-crystalline materials. J Appl Crystallogr 40:178–184

Rayment I, Holden HM, Whittaker M, Yohn M, Lorenz M, KC H, RA M (1993a) Structure of the actin-myosin complex and its implications for muscle contraction. Science 261:58–65

Rayment I, Rypniewski WR, Schmidt-Base K, Smith R, Tomchick DR, Benning MM, Winkelmann DA, Wesenberg G, Holden HM (1993b) Three-dimensional structure of myosin subfragment-1: a molecular motor. Science 261:50–58

Reedy MK (1968) Ultrastructure of insect flight muscle. I. Screw sense and structural grouping in the rigor cross-bridge lattice. J Mol Biol 31:155–176

Reedy MK, Leonard KR, Freeman R, Arad T (1981) Thick myofilament mass determination by electron scattering measurements with scanning transmission electron microscopy. J Muscle Res Cell Motil 2:45–64

Reedy et al (2016) submitted

Rome E, Offer G, Pepe FA (1973) X-ray diffraction of muscle labelled with antibody to C-protein. Nat New Biol 244:152–154

Shaffer JF, Kensler RW, Harris SP (2009) The myosin binding protein C motif binds to F-actin in a phosphorylation sensitive manner. J Biol Chem 284:12318–12327

Shoenberg CF (1969) An electron microscope study of the influence of divalent ions on myosin filament formation in chicken gizzard extracts and homogenates. Tissue Cell 1:83–96

AU5

AU6

1175 Sjostrom M, Squire JM (1977) Fine structure of the A-band in cryo-sections. The structure of the
1176   A-band of human skeletal muscle fibres from ultra-thin cryo-sections negatively stained. J Mol
1177   Biol 109:49–68
1178 Slayter HS, Lowey S (1967) Substructure of the myosin molecule as visualized by electron micros-
1179   copy. Proc Natl Acad Sci U S A 58:1611–1618
1180 Small JV, Sobieszek A (1977) Studies on the function and composition of the 10-nm (100 Å) fila-
1181   ments of vertebrate smooth muscle. J Cell Sci 23:243–268
1182 Small JV, Squire JM (1972) Structural basis of contraction in vertebrate smooth muscle. J Mol Biol
1183   67:117–149
1184 Somlyo AP, Devine CE, Somlyo AV, Rice RV (1973) Filament organization in vertebrate smooth
1185   muscle. Philos Trans R Soc Lond Ser B Biol Sci 265:223–229
1186 Squire JM (1971) General model for the structure of all myosin-containing filaments. Nature
1187   233:457–462
1188 Squire JM (1972) General model of myosin filament structure. II. Myosin filaments and cross-
1189   bridge interactions in vertebrate striated and insect flight muscles. J Mol Biol 72:125–138
1190 Squire JM (1973) General model of myosin filament structure. III. Molecular packing arrange-
1191   ments in myosin filaments. J Mol Biol 77:291–323
1192 Squire JM (1975) Muscle filament structure and muscle contraction. Annu Rev Biophys Bioeng
1193   4:137–163
1194 Squire JM (1981) The structural basis of muscular contraction. Plenum Press, New York
1195 Squire JM (1986) Muscle myosin filaments: Internal structure and crossbridge organisation.
1196   Comments Mol Cell Biophys 3:155–177
1197 Squire JM, Morris EP (1998) A new look at thin filament regulation in vertebrate skeletal muscle.
1198   FASEB J 12:761–771
1199 Squire JM, Harford JJ, Edman AC, Sjostrom M (1982) Fine structure of the A-band in cryo-
1200   sections III: crossbridge distribution and the axial structure of the human C-zone. J Mol Biol
1201   155:467–494
1202 Squire JM, Luther PK, Knupp C (2003) Structural evidence for the interaction of C-protein
1203   (MyBP-C) with actin and sequence identification of a possible actin-binding domain. J Mol
1204   Biol 331:713–724
1205 Squire JM, AL-Khayat HA, Knupp C, Luther PK (2005) 3D Molecular architecture of muscle. In
1206   'Muscle & molecular motors'. Adv Protein Chem 71: 17–87.
1207 Stewart M, Kensler RW (1986) Arrangement of myosin heads in relaxed thick filaments from frog
1208   skeletal muscle. J Mol Biol 192:831–851
1209 Stewart M, Kensler RW, Levine RJ (1981) Structure of Limulus telson muscle thick filaments.
1210   J Mol Biol 153:781–790
1211 Stewart M, Kensler RW, Levine RJ (1985) Three-dimensional reconstruction of thick filaments
1212   from Limulus and scorpion muscle. J Cell Biol 101:402–411
1213 Straussman R, Squire JM, Ben-Yaakov A, Ravid S (2005) Molecular packing of myosin II rods
1214   relates directly to the linear sequence of charged amino acids. J Mol Biol 353:613–628
1215 Szent-Györgyi AG, Cohen C, Kendrick-Jones J (1971) Paramyosin and the filaments of molluscan
1216   "catch" muscles. II. Native filaments: isolation and characterization. J Mol Biol 56:239–258
1217 Takeda S, Yamashita A, Maeda K, Maeda Y (2003) Structure of the core domain of human cardiac
1218   troponin in the Ca(2+)-saturated form. Nature 424:35–41
1219 Topf M, Lasker K, Webb B, Wolfson H, Chiu W, Sali A (2008) Protein structure fitting and refine-
1220   ment guided by cryo-EM density. Structure 6:295–307
1221 Trinick JA (1981) End-filaments: a new structural element of vertebrate skeletal muscle thick fila-
1222   ments. J Mol Biol 151:309–314
1223 Tskhovrebova L, Trinick JA (2003) Titin: properties and family relationships. Nat Rev Mol Cell
1224   Biol 4:679–689
1225 Tskhovrebova L, Trinick JA (2012) Making muscle elastic: the structural basis of myomesin
1226   stretching. PLoS Biol 10(2):e1001264

van Dijk SJ, Witt CC, Harris SP (2015) Normal cardiac contraction in mice lacking the proline-alanine rich region and C1 domain of cardiac myosin binding protein C. J Mol Cell Cardiol 88:124–132

van Heel M, Harauz G, Orlova EV, Schmidt R, Schatz M (1996) A new generation of the IMAGIC image processing system. J Struct Biol 116:17–24

van Heel M, Gowen B, Matadeen R, Orlova EV, Finn R, Pape T, Cohen D, Stark H, Schmidt R, Schatz M, Patwardhan A (2000) Single-particle electron cryo-microscopy: towards atomic resolution. Q Rev Biophys 33:307–369

Vibert PJ (1992) Helical reconstruction of frozen-hydrated scallop myosin filaments. J Mol Biol 223:661–671

Vibert PJ, Craig R (1983) Electron microscopy and image analysis of filaments from scallop striated muscle. J Mol Biol 165:303–320

Vibert PJ, Haselgrove JC, Lowy J, Poulsen FR (1972) Structural changes in actin-containing filaments of muscle. J Mol Biol 236:182–183

Vibert P, Craig R, Lehman W (1997) Steric-model for activation of muscle thin filaments. J Mol Biol 266:8–14

Vinogradova MV, Stone DB, Malanina GG, Karatzaferi C, Cooke R, Mendelson RA, Fletterick RJ (2005) Ca(2+)-regulated structural changes in troponin. Proc Natl Acad Sci U S A 102:5038–5043

von der Ecken J, Muller M, Lehman W, Manstein DJ, Penczek PA, Raunser S (2015) Structure of the F-actin-tropomyosin complex. Nature 519:114–117

Walcott S, Docken S, Harris SP (2015) Effects of cardiac myosin binding protein-C on actin motility are explained with a drag-activation-competition model. Biophys J 108:10–13

Wendt T, Taylor D, Trybus KM, Taylor K (2001) Three-dimensional image reconstruction of dephosphorylated smooth muscle heavy meromyosin reveals asymmetry in the interaction between myosin heads and placement of subfragment 2. Proc Natl Acad Sci U S A 98:165–4366

Winegrad S (2003) Myosin binding protein C (MyBP-C) in cardiac muscle and contractility. Adv Exp Med Biol 538:31–40

Whitten AE, Jeffries CM, Harris SP, Trewhella J (2008) Cardiac myosin-binding protein C decorates F-actin: implications for cardiac function. Proc Natl Acad Sci U S A 105:18360–18365

Woodhead JL, Craig R (2015) Through thick and thin: interfilament communication in muscle. Biophys J 109:665–667

Woodhead JL, Zhao FQ, Craig R, Egelman EH, Alamo L, Padrón R (2005) Atomic model of a myosin filament in the relaxed state. Nature 436:1195–1199

Woodhead JL, Zhao FQ, Craig R (2013) Structural basis of the relaxed state of a Ca2+-regulated myosin filament and its evolutionary implications. Proc Natl Acad Sci U S A 110:8561–8566

Wray JS (1979) Structure of the backbone in myosin filaments of muscle. Nature 277:37–40

Wray JS, Vibert PJ, Cohen C (1974) Cross-bridge arrangements in Limulus muscle. J Mol Biol 88:343–348

Xu J-Q, Harder BA, Uman P, Craig R (1996) Myosin filament structure in vertebrate smooth muscle. J Cell Biol 134:53–66

Xu C, Craig R, Tobacman L, Horowitz R, Lehman W (1999) Tropomyosin positions in regulated thin filaments revealed by cryoelectron microscopy. Biophys J 77:985–992

Zhao F-Q, Craig R, Woodhead JL (2009) Head–head interaction characterizes the relaxed state of Limulus muscle myosin filaments. J Mol Biol 385:423–431

Zoghbi ME, Woodhead JL, Moss RL, Craig R (2008) Three-dimensional structure of vertebrate cardiac muscle myosin filaments. Proc Natl Acad Sci U S A 105:2386–2390

Author Queries

Chapter No.: 11   0002895938

Queries	Details Required	Author's Response
AU1	Please specify "a" or "b" for Rayment et al. (1993), Elliott (1964), AL-Khayat et al. (2009).	
AU2	Hanson and Lowy (1961), Wendt et al. (1999) have been changed to (1963), Wendt et al. (2001) as per reference list. Please check if okay.	
AU3	Please confirm the caption of part figure (a) in Fig. 11.21.	
AU4	Please provide in-text citation for Trinick and Tskhovrebova (2016), Granzier and Labeit (2005), Vibert et al. (1971), Craig and Lehman (2001), Herzberg and James (1988), Labeit et al. (2011) or delete the reference from list if applicable.	
AU5	Please provide complete details for Parry (1975), Reedy et al (2016).	
AU6	Please update Paul et al. (2016).	